Knockout mouse models reveal the contributions of G protein subunits to complement C5a receptor–mediated chemotaxis

Received for publication, November 19, 2019, and in revised form, April 22, 2020 Published, Papers in Press, April 24, 2020, DOI 10.1074/jbc.RA119.011984

Esther van den Bos[1], Benjamin Ambrosy[1], Markus Horsthemke[1], Stefan Walbaum[1], Anne C. Bachg[1], Nina Wettschureck[2], Giulio Innamorati[3], Thomas M. Wilkie[4], and Peter J. Hanley[1,*]

From the [1]Institut für Molekulare Zellbiologie, Westfälische Wilhelms-Universität Münster, Münster, Germany, the [2]Department of Pharmacology, Max Planck Institute for Heart and Lung Research, Bad Nauheim, Germany, the [3]Department of Surgical Sciences, Dentistry, Gynecology and Pediatrics, University of Verona, Verona, Italy, and the [4]Department of Pharmacology, University of Texas Southwestern Medical Center, Dallas, Texas, USA

Edited by Henrik G. Dohlman

G protein–coupled receptor signaling is required for the navigation of immune cells along chemoattractant gradients. However, chemoattractant receptors may couple to more than one type of heterotrimeric G protein, each of which consists of a Gα, Gβ, and Gγ subunit, making it difficult to delineate the critical signaling pathways. Here, we used knockout mouse models and time-lapse microscopy to elucidate Gα and Gβ subunits contributing to complement C5a receptor-mediated chemotaxis. Complement C5a-mediated chemokinesis and chemotaxis were almost completely abolished in macrophages lacking *Gnai2* (encoding Gα_{i2}), consistent with a reduced leukocyte recruitment previously observed in *Gnai2*$^{-/-}$ mice, whereas cells lacking *Gnai3* (Gα_{i3}) exhibited only a slight decrease in cell velocity. Surprisingly, C5a-induced Ca^{2+} transients and lamellipodial membrane spreading were persistent in *Gnai2*$^{-/-}$ macrophages. Macrophages lacking both *Gnaq* (Gα_q) and *Gna11* (Gα_{11}) or both *Gna12* (Gα_{12}) and *Gna13* (Gα_{13}) had essentially normal chemotaxis, Ca^{2+} signaling, and cell spreading, except *Gna12*/*Gna13*-deficient macrophages had increased cell velocity and elongated trailing ends. Moreover, *Gnaq*/*Gna11*-deficient cells did not respond to purinergic receptor $P2Y_2$ stimulation. Genetic deletion of *Gna15* (Gα_{15}) virtually abolished C5a-induced Ca^{2+} transients, but chemotaxis and cell spreading were preserved. Homozygous *Gnb1* (Gβ_1) deletion was lethal, but mice lacking *Gnb2* (Gβ_2) were viable. *Gnb2*$^{-/-}$ macrophages exhibited robust Ca^{2+} transients and cell spreading, albeit decreased cell velocity and impaired chemotaxis. In summary, complement C5a-mediated chemotaxis requires Gα_{i2} and Gβ_2, but not Ca^{2+} signaling, and membrane protrusive activity is promoted by G proteins that deplete phosphatidylinositol 4,5-bisphosphate.

The study of immune cell chemotaxis dates back to 1888 (1), when the German ophthalmologist Th. Leber (Theodor Karl Gustav Leber), using a model of mycotic keratitis, observed the migration of leukocytes to sites of inflammation, where they accumulated in large numbers, reminiscent of the swarming of neutrophils to injured tissue described more recently by Lämmermann *et al.* (2). Gradients of chemoattractant ligands emanating from sites of inflammation or injured tissue guide cells by binding to G protein–coupled receptors (GPCRs), but how spatiotemporal ligand-GPCR signaling accomplishes this has not been delineated. *Dictyostelium discoideum* has proven to be a good model system for the study of chemotaxis (3), leading to the development of the LEGI (local excitation, global inhibition) model (4) and more complex excitable network hypotheses (5). In contrast to *Dictyostelium* amoebae, mammalian chemoattractant receptors, such as the complement C5a receptor (C5aR), may activate more than one type of heterotrimeric G protein (6–8), which adds considerable complexity to the signal transduction. Nevertheless, the G$\alpha_{i/o}$ family has been strongly implicated in chemotactic signaling because pertussis toxin (PTX; previously known as lymphocytosis-promoting factor) from *Bordetella pertussis*, which blocks the activation of G$\alpha_{i/o}$ subunits by GPCRs, inhibits the chemotaxis of macrophages and other phagocytes (9–11). Moreover, the recruitment of neutrophils and macrophages to inflamed lung or peritoneum is decreased by around 50% in mice lacking *Gnai2*, which encodes Gα_{i2} (12, 13).

Genetic deletion of *Gna15*, a hemopoietic-specific gene coding for the Gα_q/Gα_{11} family member Gα_{15}, markedly decreases complement C5a-induced Ca^{2+} transients in macrophages (14), but the role of Gα_{15} in complement C5a-mediated chemotaxis has not been determined. The other members of the Gα_q/Gα_{11} family are encoded by *Gnaq* (Gα_q) and *Gna11* (Gα_{11}), respectively, in mouse, but the roles of these subunits in chemotaxis are unclear. In cotransfection studies, the chemokine (chemotactic cytokine) receptors for CCL2 (chemokine (CC motif) ligand 2; also known as monocyte chemoattractant protein-1) and CCL5 (also known as RANTES (regulated on activation, normal T cell expressed and secreted)) were shown to couple to Gα_q (6). In contrast, CXCL8 (chemokine (CXC motif) ligand 8; also known as interleukin-8) and complement C5a did not activate Gα_q (6). However, complement C5a may indirectly couple to Gα_q and/or Gα_{11} through C5aR-induced autocrine ATP signaling that activates purinergic receptors (15, 16).

This article contains supporting information.

* For correspondence: Peter J. Hanley, hanley@uni-muenster.de.

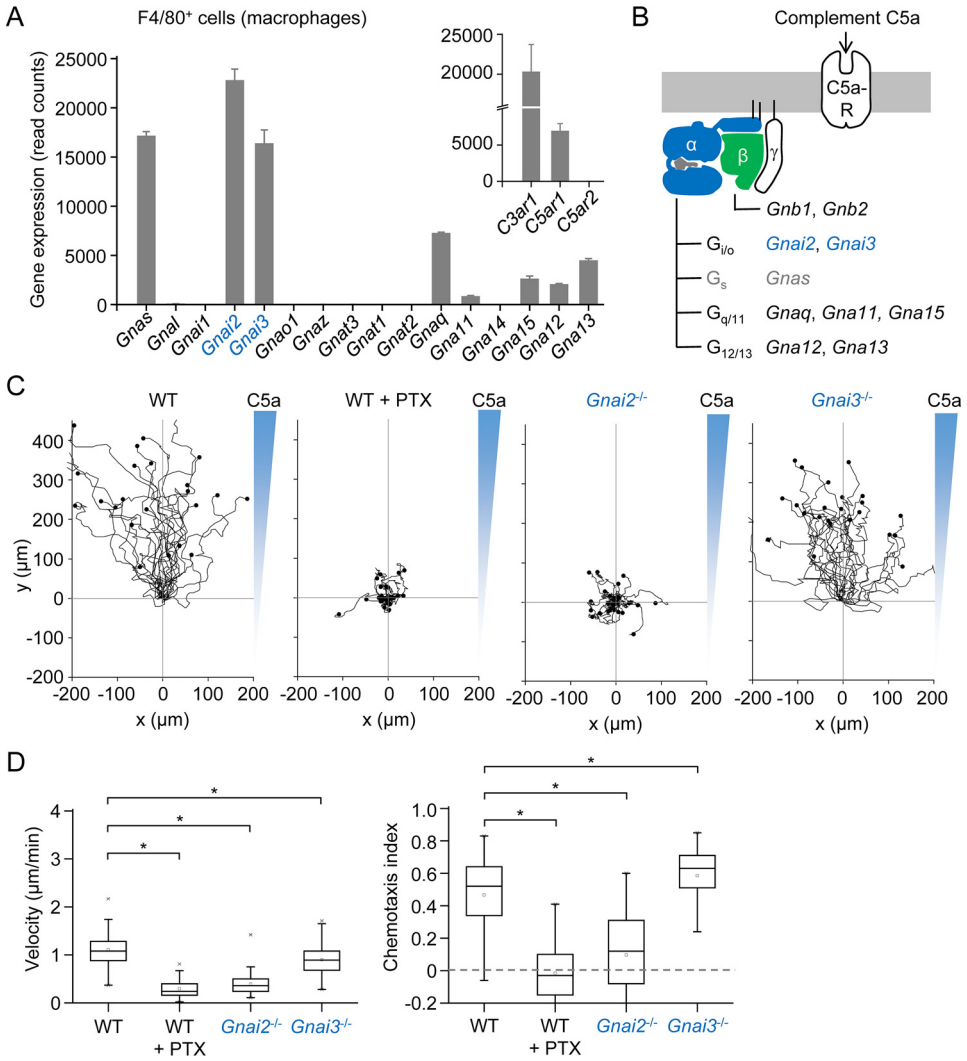

Figure 1. Expression of Gα subunits in macrophages and roles of *Gnai2* and *Gnai3* in complement C5a-mediated chemotaxis. *A*, expression levels of Gα subunits in mouse resident peritoneal F4/80$^+$ cells (macrophages). RNA-Seq analysis was performed using RNA isolated from resident peritoneal F4/80$^+$ cells purified by cell sorting ($n = 3$ mice). *Inset* (superimposed graph with an interrupted *y* axis), expression levels of receptors for complement components 3a and 5a. *Error bars*, S.E. *B*, schematic diagram showing C5aR, a member of the G protein–coupled receptor superfamily, and a heterotrimeric G protein in which the subunits are *color-coded blue* (Gα), *green* (Gβ), and *white* (Gγ). The four Gα families (G$\alpha_{i/o}$, Gα_s, G$\alpha_{q/11}$, and G$\alpha_{12/13}$) are listed *below* the *blue* α-subunit (Gα) together with the names of the corresponding genes investigated with knockout mouse models, including two genes encoding β-subunits: *Gnb1* (Gβ_1) and *Gnb2* (Gβ_2). *C*, migration plots of WT, PTX-treated WT, *Gnai2*$^{-/-}$, and *Gnai3*$^{-/-}$ macrophages in a chemotactic complement C5a gradient. *D*, summary box plots of cell velocity and chemotactic efficiency (chemotaxis index), calculated by dividing the displacement along the *y* axis by the cumulative distance migrated. The chemotaxis index is also known as the *y*-forward migration index and has a range of -1 to $+1$. *, $p < 0.05$; Kruskal–Wallis test and post hoc Mann–Whitney *U* test with Bonferroni correction ($n = 75$ for each group, except $n = 50$ for the WT + PTX group; three independent experiments, except two independent experiments for the WT + PTX group).

In this study, we used knockout mouse models to explore the roles of different G protein subunits in macrophage chemotaxis. More specifically, we used time-lapse microscopy to visualize the navigation and movement of macrophages, isolated from WT or various knockout mice, in a chemotactic complement C5a gradient, and, in parallel, we imaged the Ca^{2+} signaling and lamellipodial membrane dynamics in individual cells upon C5aR stimulation.

Results

Gnai2, but not Gnai3, is critical for complement C5a-mediated chemotaxis

RNA sequence analysis of purified resident peritoneal F4/80$^+$ cells (macrophages) revealed that *Gnai2* (Gα_{i2}) and *Gnai3* (Gα_{i3}) of the G$\alpha_{i/o}$ family of Gα-subunits, as well as *Gnas* (Gα_s) and members of the Gα_q/Gα_{11} (*Gnaq*, *Gna11*, and *Gna15*) and Gα_{12}/Gα_{13} (*Gna12* and *Gna13*) families, are expressed, as well as complement C5a receptor 1 (as known as CD88), encoded by *C5ar1* (Fig. 1, *A* and *B*). Notably, the controversial C5aR, complement C5a receptor 2 (17), encoded by *C5ar2*, was negligibly expressed (see the *inset* with interrupted *y* axis in Fig. 1*A*). We used knockout mouse models to explore the roles of the various Gα and Gβ subunits shown in Fig. 1*B*, except *Gnas* (Gα_s), in transducing gradients of the chemoattractant complement C5a into stimulated motility (chemokinesis) and directed cell migration (chemotaxis) using the μ-Slide Chemotaxis chamber (16, 18) and time-lapse, phase-contrast microscopy. Macrophages isolated from WT mice migrated robustly along chemotactic gradients of complement C5a (Fig. 1*C* and Videos S1 and S2). Incubation with PTX (1 μg/ml),

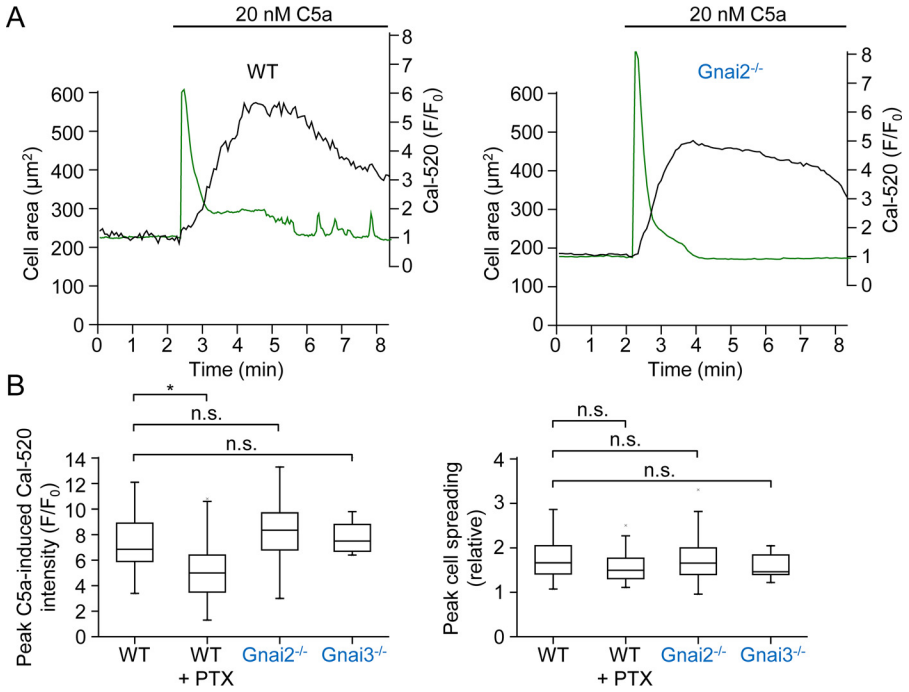

Figure 2. Complement C5a-induced Ca^{2+} transients and lamellipodial membrane protrusions are not impaired in *Gnai2*$^{-/-}$ or *Gnai3*$^{-/-}$ macrophages. *A*, simultaneous imaging of intracellular [Ca^{2+}] (*green trace*) and projected cell area (*black trace*) in individual WT and *Gnai2*$^{-/-}$ macrophages challenged with 20 nM complement C5a. Intracellular [Ca^{2+}] is indexed as relative Cal-510 fluorescence intensity (F/F_0) in which the measured fluorescence intensity (*F*) is divided by the resting fluorescence intensity (F_0) after subtracting the background fluorescence intensity at each time point. *B*, summary box plots of peak complement C5a-induced Ca^{2+} transients and projected cell area. *, $p < 0.05$; *n.s.*, not significant; Kruskal–Wallis test and post hoc Mann–Whitney *U* test with Bonferroni correction ($n = 50$ (WT), $n = 19$ (WT + PTX), $n = 46$ (*Gnai2*$^{-/-}$), and $n = 9$ (Gnai3$^{-/-}$); 2–3 independent experiments).

which ADP-ribosylates a serine residue and inhibits $G\alpha_{i2}$ and $G\alpha_{i3}$ as well as other $G\alpha_{i/o}$ family members (19), abolished complement C5a-mediated chemokinesis and chemotaxis (Fig. 1*C*). Similarly, genetic deletion of *Gnai2* markedly impaired cell velocity and chemotactic navigation in a complement C5a gradient (Fig. 1 (*C* and *D*) and Videos S3–S6), whereas deletion of *Gnai3* only marginally impaired cell velocity. The extent of *in vitro* chemotaxis impairment in *Gnai2*$^{-/-}$ macrophages was greater than expected when compared with WT *versus* *Gnai2*$^{-/-}$ mouse *in vivo* inflammation models (12, 13).

Complement C5a-induced Ca^{2+} transients and lamellipodial cell spreading are intact in Gnai2-deficient macrophages

We have previously shown that complement C5a induces robust Ca^{2+} transients (20), which are monophasic at high agonist concentrations, and lamellipodial cell spreading in mouse macrophages (21). In the following experiments, we simultaneously imaged intracellular [Ca^{2+}], using the fluorescent Ca^{2+} indicator Cal-520, and membrane dynamics, assessed by brightfield microscopy (Fig. 2). Macrophages, like neutrophils, migrate on a two-dimensional surface in an amoeboid fashion in which the dominant lamellipodial membrane protrusion steers the cell (22, 23) and in the case of chemotaxis needs to be directed toward higher concentrations of chemoattractant (24), as evident, for example, in Video S1. We therefore tested whether complement C5a-induced lamellipodial membrane protrusive activity is defective in *Gnai2*$^{-/-}$ macrophages. Surprisingly, similar to WT macrophages, complement C5a induced robust monophasic Ca^{2+} transients and lamellipodial membrane protrusions in the absence of *Gnai2* (Fig. 2*A* and Videos S7 and S8). Deletion of either *Gnai2* or *Gnai3* did not significantly decrease the peak levels of complement C5a-induced Ca^{2+} transients or cell spreading, indexed as the peak projected cell area normalized to that preceding stimulation (Fig. 2*B*). The Ca^{2+} transient peak, but not peak cell spreading, was decreased by PTX treatment (Fig. 2*B*).

The temporal relation between complement C5a-induced Ca^{2+} transients and cell spreading suggested that rapid increases in intracellular [Ca^{2+}] may promote branched actin polymerization, which drives lamellipodial membrane extension. To test this notion, we loaded the cytosol of macrophages with the Ca^{2+} chelator EGTA, using its cell-permeable acetoxymethyl (AM) ester form (EGTA/AM). Intracellular loading of cells with EGTA almost completely abolished complement Ca^{2+}-induced Ca^{2+} transients (Fig. 3*A*), but cell spreading was not abrogated (Fig. 3*B*). This implies that the second messenger Ca^{2+} is not important for the formation of complement C5a-induced lamellipodial membrane protrusions.

Double Gnaq/Gna11 or Gna12/Gna13 knockout macrophages have robust complement C5a-mediated chemotaxis

Next, we investigated the roles of the $G\alpha_q/G\alpha_{11}$ and $G\alpha_{12}/G\alpha_{13}$ families of $G\alpha$ subunits (schematically illustrated in Fig. 4*A*) in complement C5a-mediated chemotaxis using triple mutant mice in which one gene is deleted and the second one is conditionally knocked out in myeloid cells, which includes macrophages. The median velocity and chemotaxis index of macrophages isolated from *Gnaq*$^{fl/fl}$/LysM-Cre/*Gna11*$^{-/-}$ (*Gnaq*/*Gna11* dKO (double knockout)) mice, in which *Gna11* is constitutively deleted and *Gnaq* is conditionally deleted, did

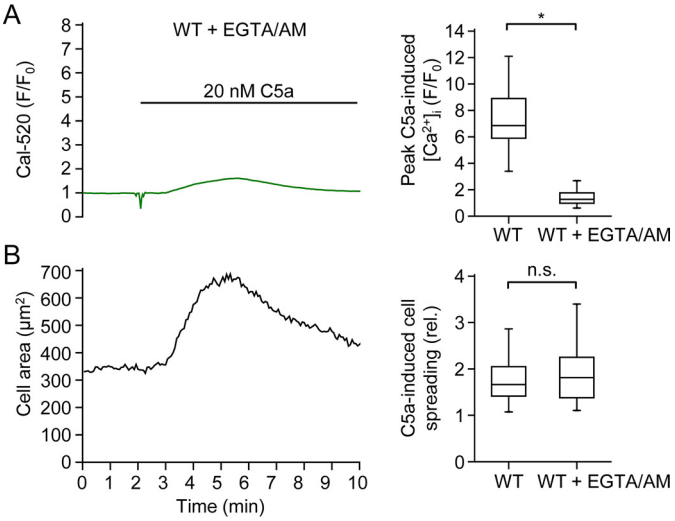

Figure 3. Sequestration of intracellular [Ca^{2+}] with EGTA does not prevent complement C5a-induced lamellipodial membrane protrusions. *A*, example (green trace) of a complement C5a-induced Ca^{2+} transient largely blocked in a WT macrophage after passively loading the cell with the Ca^{2+} chelator EGTA using its AM ester form (EGTA/AM). The box plots on the *right* show peak complement C5a-induced Ca^{2+} transients measured in the absence and presence of EGTA/AM. *B*, the trace shows the projected cell area corresponding to the above Ca^{2+} trace (*A*). The box plots on the *right* show peak complement C5a-induced cell spreading in the absence and presence of EGTA/AM. *, $p < 0.05$; *n.s.*, not significant; Mann–Whitney *U* test ($n = 50$ (WT pool) and $n = 43$ (WT + EGTA/AM); $n = 3$ independent experiments).

not differ from the values for WT macrophages (Fig. 4*B*). Similarly, macrophages isolated from *Gna12*$^{-/-}$/*Gna13*$^{fl/fl}$/LysM-Cre (*Gna12*/*Gna13* dKO) mice, in which *Gna12* is deleted and *Gna13* is conditionally deleted, clearly navigated well along chemotactic complement C5a gradients, although the median velocity of *Gna12*/*Gna13* dKO macrophages was modestly increased (Fig. 4, *B* and *C*). The polarized morphology of *Gnaq*/*Gna11* dKO macrophages migrating in a complement C5a gradient was unremarkable (Videos S9 and S10), whereas *Gna12*/*Gna13* dKO macrophages exhibited modestly elongated trailing ends (Fig. 4*D* and Videos S11 and S12), reminiscent of the phenotype of conditional *Rhoa* knockout macrophages (25), but much less extreme than *Rhoa*/*Rhob* double knockout macrophages (25). Measurements of maximal tail length (Fig. 4, *D* and *E*), assessed over a 6-h migration period, confirmed that *Gna12*/*Gna13* dKO macrophages developed elongated trailing ends (Fig. 4*E*). The modest phenotypes of *Gna12*/*Gna13* dKO macrophages suggest that complement C5a coupling to $G\alpha_{12}$ and $G\alpha_{13}$ contributes to the activation of the Rho subfamily of Rho GTPases and retraction of the trailing end in migrating cells. Consistent with this interpretation, we found that application of complement C5a increased the levels of active RhoA (RhoA-GTP) in WT mouse bone marrow–derived macrophages, measured by G-LISA assays (Fig. 4*F*).

UTP-induced Ca^{2+} transients are largely abolished in Gnaq/Gna11 double knockout macrophages

Extracellular UTP and ATP induce large Ca^{2+} transients in mouse macrophages by binding to $P2Y_2$ receptors ($P2Y_2$Rs), although ATP additionally induces Ca^{2+} influx via P2X receptors, ATP-gated, nonselective cation channels (20). $P2Y_2$Rs are thought to signal to $G\alpha_q$ and $G\alpha_{11}$ (26, 27), functionally similar G proteins that are typically not distinguished by receptors (8). Indeed, we found that UTP-induced Ca^{2+} signaling was almost completely abrogated in *Gnaq*/*Gna11* dKO macrophages, whereas subsequent application of complement C5a induced robust Ca^{2+} transients (Fig. 5, *A* and *B*). Note that the decaying Ca^{2+} hump following large complement C5a-induced Ca^{2+} peaks can be explained by store-operated Ca^{2+} entry because it is absent in Ca^{2+}-free media and can be evoked by reintroduction of Ca^{2+}-containing media (20). The large complement C5a-induced Ca^{2+} peak persists in Ca^{2+}-free media and is produced by endoplasmic reticular (ER) Ca^{2+} release (20).

Unlike $G\alpha_q$ and $G\alpha_{11}$, which stimulate phospholipase C-β (PLC-β) activity and generate the ER Ca^{2+}-releasing agonist inositol 1,4,5-trisphosphate (IP_3) via phosphatidylinositol 4,5-bisphosphate (PIP_2) hydrolysis, $G\alpha_{12}$ and $G\alpha_{13}$ do not stimulate PLC-β, but instead activate Rho guanine nucleotide exchange factors (RhoGEFs). Thus, complement C5a signaling to $G\alpha_{12}$ and $G\alpha_{13}$ is unlikely to shape the Ca^{2+} response. Indeed, complement C5a induced robust Ca^{2+} transients in *Gna12*/*Gna1*3 dKO macrophages (Fig. 6, *A* and *B*). There were no significant differences in the peak Ca^{2+} responses of *Gna12*/*Gna13* dKO or *Gnaq*/*Gna11* dKO macrophages compared with WT cells (Fig. 6*C*). Moreover, complement C5a induced lamellipodial membrane spreading in both *Gnaq*/*Gna11* dKO and *Gna12*/*Gna13* dKO macrophages, such that median cell area significantly increased by 1.5-fold ($n = 25$; three independent experiments) and 1.4-fold ($n = 17$; two independent experiments), respectively.

Gna15$^{-/-}$ macrophages have intact chemotaxis, but complement C5a-induced Ca^{2+} signaling is largely abolished

To determine whether the hematopoietic-restricted α-subunit $G\alpha_{15}$, a member of the $G\alpha_q$/$G\alpha_{11}$ family (as illustrated in Fig. 7*A*), is required for macrophage migration toward complement C5a, we performed real-time chemotaxis assays. Similar to WT cells, *Gna15*$^{-/-}$ macrophages migrated efficiently along complement C5a gradients (Fig. 7*B* and Videos S13 and S14), and cells showed normal polarized morphologies in a chemotactic gradient (Fig. 7*C* and Videos S13 and S14). There were no significant differences in the measured velocity and chemotactic efficiency of WT and *Gna15*$^{-/-}$ macrophages migrating in a complement C5a gradient (Fig. 7*D*).

Davignon *et al.* (14) showed that *Gna15* is not required for normal hematopoiesis but found that complement C5a-induced Ca^{2+} transients, averaged from at least five cells, were markedly decreased in thioglycolate-elicited peritoneal macrophages from *Gna15*$^{-/-}$ mice, whereas responses to ATP or UTP were similar to WT macrophages. In accord with the findings of Davignon *et al.* (14), we found that WT resident peritoneal macrophages produced robust Ca^{2+} transients upon application of complement C5a, as well as 10 min later following the application of UTP (Fig. 8*A*), whereas most individual *Gna15*$^{-/-}$ macrophages did not respond to complement C5a and those that responded gave a weak signal (Fig. 8, *B* and *C*). The peak intracellular Ca^{2+} response to

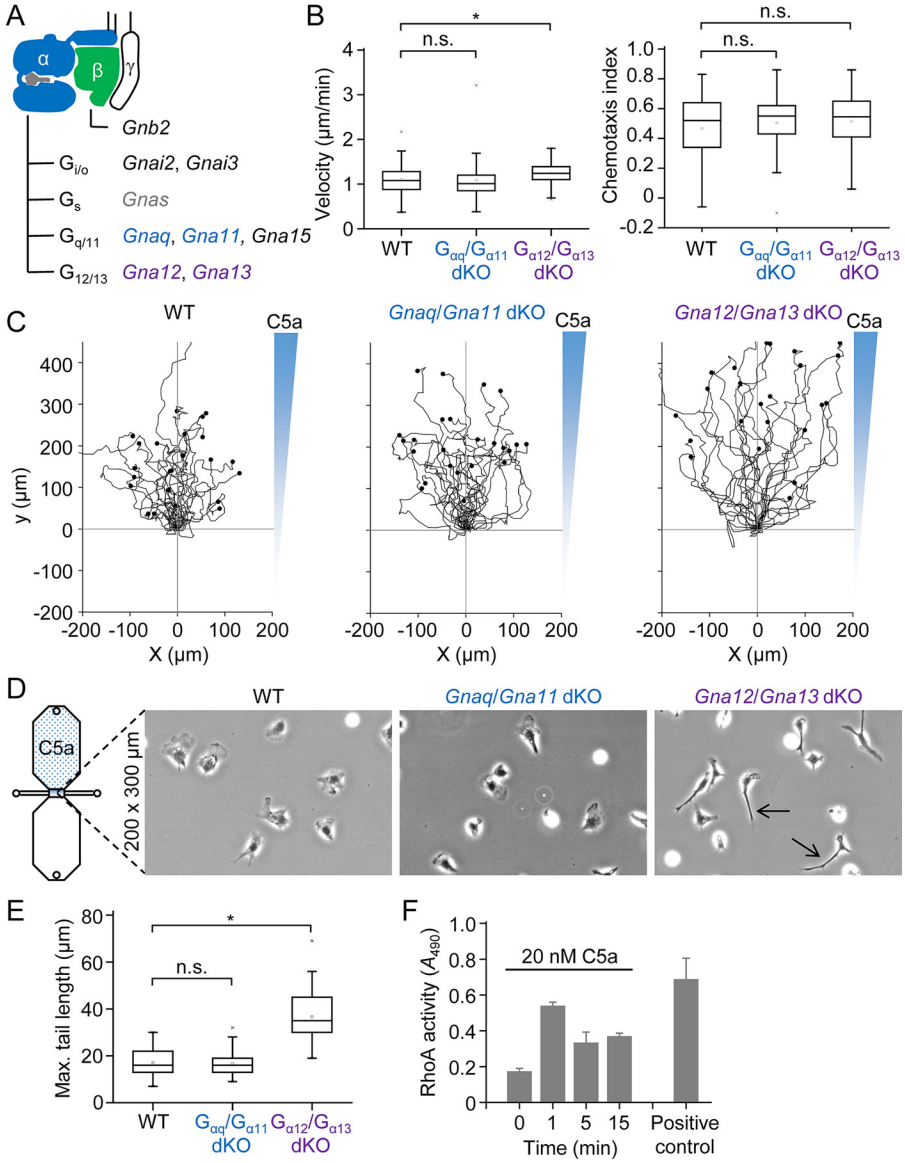

Figure 4. Complement C5a-mediated chemotaxis is preserved in *Gnaq*/*Gna11* double knockout and *Gna12*/*Gna13* double knockout macrophages. *A*, schematic diagram highlighting genes of the $G\alpha_q/G\alpha_{11}$ (*Gnaq* and *Gna11*) and $G\alpha_{12}/G\alpha_{13}$ (*Gna12* and *Gna13*) families of Gα subunits that potentially may be activated by C5aR. *B*, summary box plots of cell velocity and chemotactic efficiency (chemotaxis index). *$p < 0.05$; Kruskal–Wallis test and post-hoc Mann–Whitney *U* test with Bonferroni correction ($n = 75$ for each group; 3 independent experiments). *C*, migration plots of WT, *Gnaq*/*Gna11* dKO, and *Gna12*/*Gna13* dKO macrophages in a chemotactic complement C5a gradient. *D*, 200 × 300-μm snapshots of WT, *Gnaq*/*Gna11* dKO, and *Gna12*/*Gna13* dKO macrophages in a chemotactic complement C5a gradient. *Black arrows*, elongated trailing ends. The schematic diagram on the *left* shows a μ-Slide Chemotaxis chamber with one of the two 40-μl reservoirs (filled with a *blue dotted pattern*) containing 20 nM complement C5a. *E*, box plots of maximal tail lengths developed by macrophages migrating in a chemotactic complement C5a gradient over a 6-h period. *, $p < 0.05$; Kruskal–Wallis test and post hoc Mann–Whitney *U* test with Bonferroni correction ($n = 50$ cells/group; sampled from two independent experiments). *F*, representative example, from two independent experiments, of RhoA activity measured using a colorimetric G-LISA assay, in which active RhoA (RhoA-GTP) was indexed as absorbance at 490 nm (A_{490}). RhoA protein was used as positive control. *Bars*, mean ± S.D. (*error bars*) of duplicate measurements.

UTP 10 min after complement C5a application was significantly weaker in WT macrophages compared with *Gna15*$^{-/-}$ macrophages (Fig. 8*C*). This could possibly be explained as follows. The large cytosolic Ca^{2+} signal induced by complement C5a in WT cells (which is virtually absent in *Gna15*$^{-/-}$ cells) causes inactivation of ER Ca^{2+} release channels (IP_3 receptors), which has been shown to occur after ~30 s in the sustained presence of IP_3 (28). Thus, the weaker response to the second agonist (UTP) probably reflects insufficient resensitization of these channels and/or other factors, such as insufficient time for replenishment of ER Ca^{2+} stores and membrane PIP_2 levels.

Complement C5a-induced lamellipodial membrane protrusions are preserved in Gna15$^{-/-}$ *macrophages*

We next tested whether impaired lamellipodial cell spreading accompanied the loss of Ca^{2+} signaling in *Gna15*$^{-/-}$ macrophages. Instead of using transmitted light on the spinning disk confocal microscope to assess membrane dynamics, as in earlier experiments, we used the fluorescent plasma membrane stain CellMask Orange. This fluorophore nicely stained the membrane of macrophages, but it also weakly labeled the surface of fibronectin-coated μ-Slide I chambers (Fig. 9*A*). Application of complement C5a induced rapid and robust lamellipodial membrane protrusions in WT (Fig. 9*A* and Video

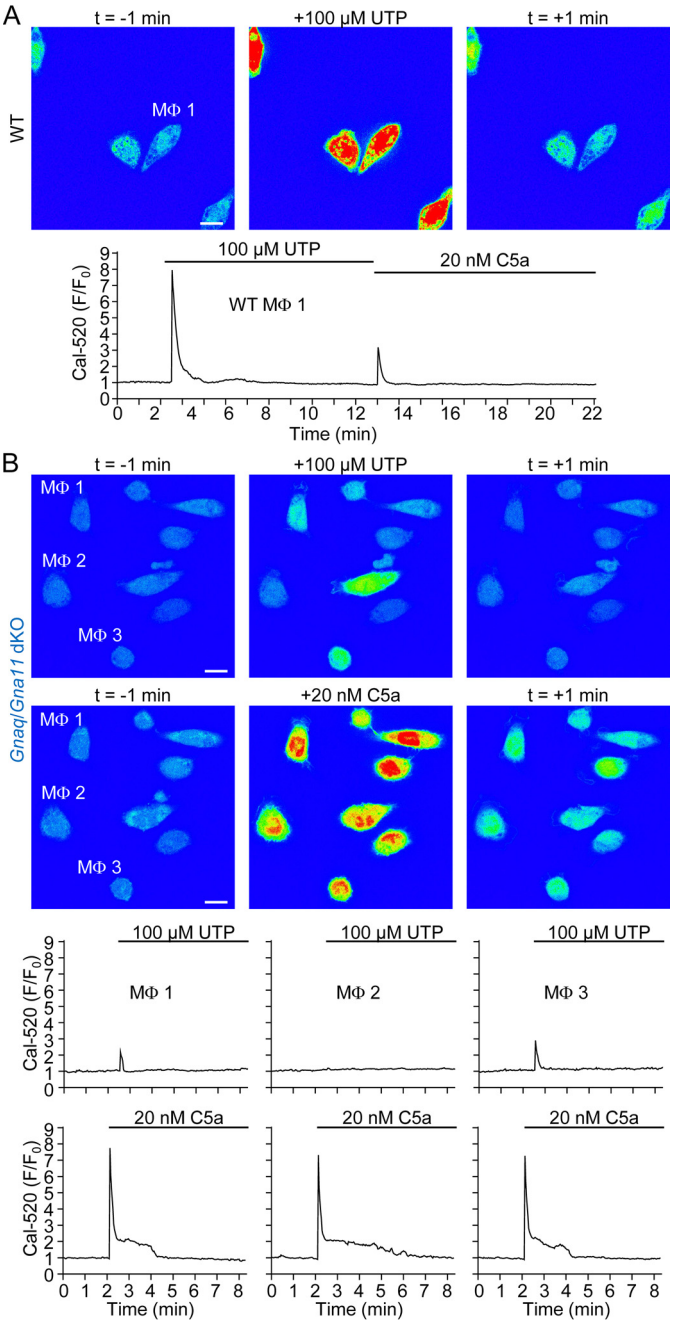

Figure 5. UTP- and complement C5a-induced Ca^{2+} transients in *Gnaq/Gna11* double knockout macrophages. *A*, time-lapse images (90 × 90 μm) of WT macrophages loaded with the fluorescent Ca^{2+} indicator Cal-520. UTP was added as indicated. *Scale bar*, 10 μm. The intracellular Ca^{2+} signaling corresponding to the labeled macrophage (*MΦ1*) is shown *below*. Intracellular [Ca^{2+}] is indexed as relative Cal-520 fluorescence intensity (F/F_0), where the measured fluorescence intensity (F) is divided by the resting fluorescence intensity (F_0) after subtracting the background fluorescence intensity at each time point. *B*, time-lapse images (90 × 90 μm) of *Gnaq/Gna11* dKO macrophages loaded with the fluorescent Ca^{2+} indicator Cal-520. UTP was added as indicated, and 22 min later, complement C5a was applied to the same cells. *Scale bars*, 10 μm. The intracellular Ca^{2+} signals corresponding to the labeled macrophages (*MΦ1*, *MΦ2*, and *MΦ3*) are shown *below*.

S15) and *Gna15*$^{-/-}$ macrophages (Fig. 9*A* and Video S16). Fig. 9*A* shows snapshots of CellMask Orange recordings, whereas the supporting videos (Videos S15 and S16) show an overlay of fluorescent Cal-520 and CellMask Orange signals. A sharp increase in intracellular [Ca^{2+}] precedes cell spreading in WT macrophages (Video S15), whereas no increase in intracellular [Ca^{2+}] is seen in *Gna15*$^{-/-}$ macrophages (see the Cal-520 fluorescence intensity trace in Fig. 9*A* and Video S16). Notably, in Fig. 9*A* and in the accompanying video (Video S15), the introduction of complement C5a-containing medium to WT macrophages caused a marginal shift of the focal plane in the *z* axis. Quantification of the images confirmed that complement C5a induced significant increases in projected cell area in both WT and *Gna15*$^{-/-}$ macrophages (Fig. 9*B*), and the effects could not be explained by effects of shear stress (Fig. 9*C*), which typically causes ruffling with minimal net cell spreading. There was no difference, WT *versus* *Gna15*$^{-/-}$ macrophages, in the magnitude of complement C5a-induced cell spreading (Fig. 9*D*).

Gnb1 and Gnb2 knockout mouse models generated using CRISPR/Cas9

Impaired inflammation-mediated phagocyte recruitment in *Gnai2*$^{-/-}$ mice (12, 13) and real-time chemotaxis assays using macrophages isolated from *Gnai2*$^{-/-}$ mice (see Fig. 1) strongly implicate $G\alpha_{i2}$ as a central signal transducer in chemotactic complement C5a signaling. In addition to the inhibitory effect of $G\alpha_i$ subunits on adenylyl cyclase, the $G\beta\gamma$ subunits released upon activation of members of the $G\alpha_{i/o}$ family are known to regulate various signal pathways, including PLC-β isoforms, phosphoinositide 3-kinases (PI3Ks), and ion channels (8). PI3Ks catalyze the conversion of PIP_2 to phosphatidylinositol 3,4,5-trisphosphate (PIP_3), a key phospholipid implicated in chemotactic signaling (3). $G\beta$ subunits are encoded by five genes in mice (*Gnb1–5*), and RNA sequence analysis revealed that *Gnb1* and *Gnb2* are predominantly expressed in macrophages (Fig. 10*A*). *Gnb1* and *Gnb2* (schematically illustrated in Fig. 10*B*) have been implicated in chemotaxis in knockdown studies using the mouse macrophage cell line J774A.1 (29, 30). Recently, the Knockout Mouse Phenotyping Program (KOMP^2) (31) generated *Gnb1* and *Gnb2* knockout mice using CRISPR/Cas9. Homozygous deletion of *Gnb1* was lethal, assessed at postnatal days 13–14 (Fig. 10*C*), consistent with the study by Okae and Iwakura (32) in which *Gnb1* was disrupted by gene trap mutagenesis. Targeted deletion of *Gnb2* was not lethal (Fig. 10*D*). The deletion allele, the location of primer binding sites, and an example of PCR genotyping are shown in Fig. 10*E*. In addition to the loss of exons 3–4, the 359-bp deletion mediated by guide RNAs and Cas9 introduces a frameshift and premature termination codon.

Gnb2$^{-/-}$ macrophages exhibited robust lamellipodial membrane spreading in response to the application of complement C5a (Fig. 11*A* and Video S17). Moreover, the peaks of complement C5a-induced cell spreading and Ca^{2+} transients (examples are shown in the *bottom panels* of Fig. 11*A*), indexed as Cal-520 fluorescence, were not significantly different compared with controls (see summary box plots in Fig. 11*B*).

Finally, we looked at the role of $G\beta_2$-containing $\beta\gamma$-subunits (schematically illustrated in Fig. 12*A*) in complement C5a-mediated chemotaxis. Compared with WT macrophages migrating in a complement C5a gradient, *Gnb2*-deficient macrophages showed reduced velocity and impaired chemotactic

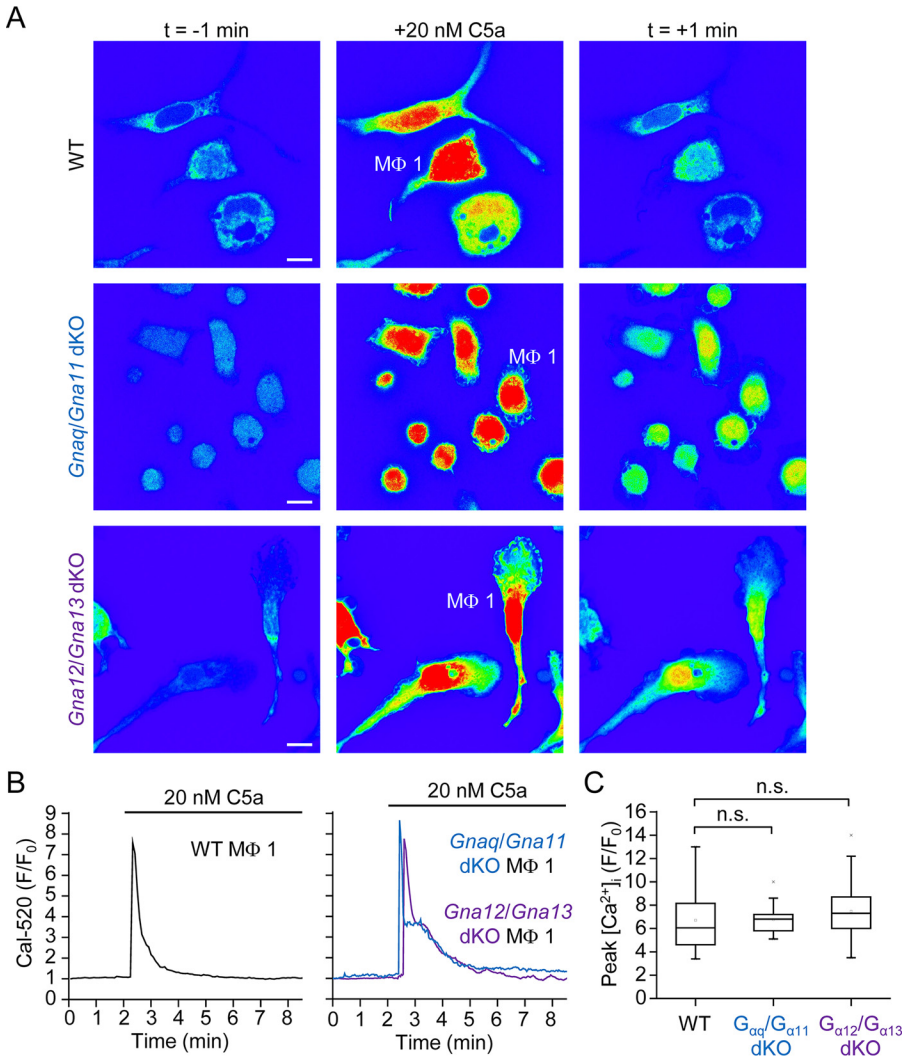

Figure 6. Intact complement C5a-induced Ca^{2+} transients in *Gna12/Gna13* double knockout and *Gnaq/Gna11* double knockout macrophages. *A*, time-lapse images (90 μm × 90 μm) of WT, *Gnaq/Gna11* dKO, and *Gna12/Gna13* dKO macrophages loaded with the fluorescent Ca^{2+} indicator Cal-520. Complement C5a was added as indicated. *Scale bars*, 10 μm. *B*, intracellular Ca^{2+} signals corresponding to the above labeled macrophages (MΦs; *A*). Intracellular [Ca^{2+}] is indexed as relative Cal-520 fluorescence intensity (F/F_0), where the measured fluorescence intensity (F) is divided by the resting fluorescence intensity (F_0) after subtracting the background fluorescence intensity at each time point. *C*, summary peak [Ca^{2+}] data. *n.s.*, not significant; Kruskal–Wallis test (n = 20–27 per group; 2–3 independent experiments).

navigation (Fig. 12*B*). *Gnb2*$^{-/-}$ macrophages polarized in the presence of complement C5a (Fig. 12*C*), but lamellipodial membrane protrusions were less efficiently directed toward higher concentrations of complement C5a (Videos S18 and S19). Summary data are plotted in Fig. 12*D*. Both cell velocity and chemotactic efficiency were significantly decreased in *Gnb2*$^{-/-}$ macrophages compared with WT controls.

Discussion

Intravital imaging, dating back to 1888, provides insight into the behavior of immune cells in their natural environment, but using this approach, it has been difficult to study the chemotactic response of cells to a specific molecule. This problem was solved by the introduction of the Boyden chamber (33), consisting of two reservoirs separated by a thin membrane. However, in Boyden-type transwell assays, the cells only move across a thin membrane, typically with a thickness of about 10 μm, making it difficult to assess cell morphology and to distinguish chemokinesis from chemotaxis. Using knockout mouse models and real-time chemotaxis assays, which allow visualization of cell morphology and measurement of cell velocity and chemotactic efficiency, we investigated the roles of specific G protein subunits ($G\alpha_{i2}$, $G\alpha_{i3}$, $G\alpha_q/G\alpha_{11}$, $G\alpha_{12}/G\alpha_{13}$, $G\alpha_{15}$, $G\beta_1$, and $G\beta_2$) in transducing complement C5a gradients to directed migration. The specific inhibitor of $G\alpha_{i/o}$ subunits pertussis toxin abrogated complement C5a-mediated chemokinesis and chemotaxis, which was largely recapitulated in *Gnai2* ($G\alpha_{i2}$) knockout macrophages, whereas *Gnai3* ($G\alpha_{i3}$) mutants exhibited robust chemotactic efficiency but marginally reduced cell velocity. Thus, $G\alpha_{i2}$ is a cornerstone of complement C5a-mediated chemotaxis, schematically illustrated in Fig. 13. However, *Gnai2*$^{-/-}$ macrophages, as well as WT macrophages treated with pertussis toxin, still induced robust Ca^{2+} transients and lamellipodial membrane protrusions upon stimulation with complement C5a. Thus, $G\alpha_{i2}$ is not essential for the generation of membrane protrusions, but it is indispens-

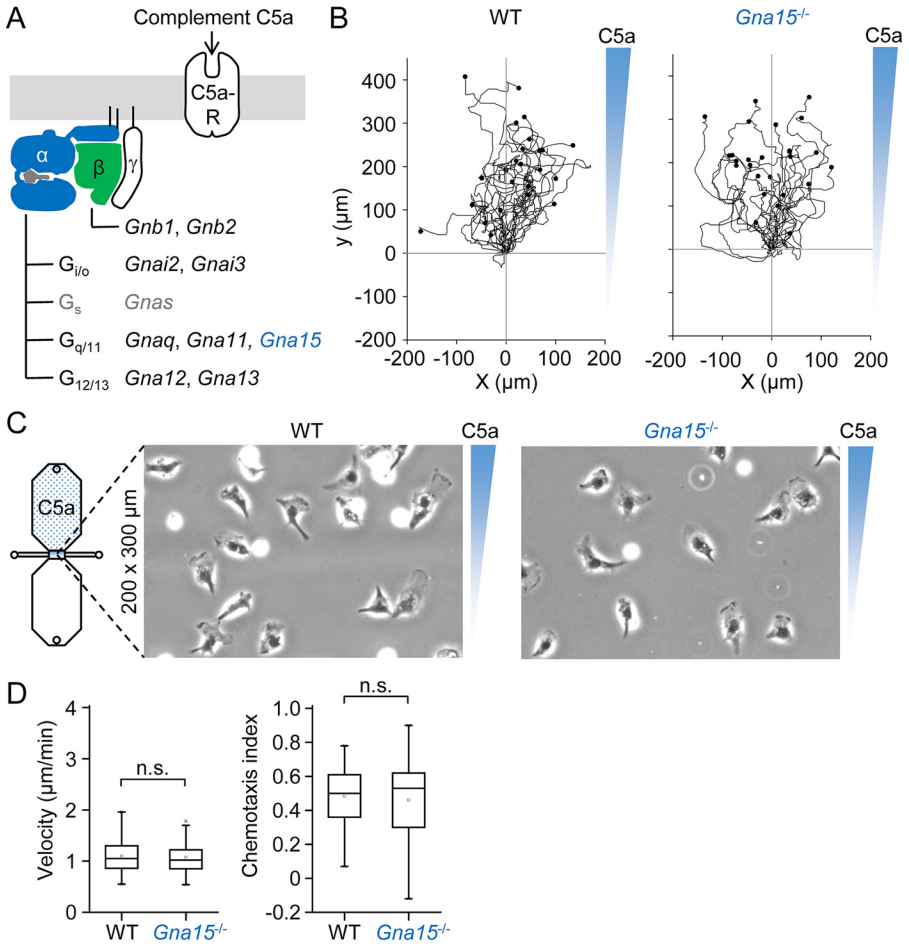

Figure 7. Gna15 is redundant for complement C5a-mediated chemotaxis. *A*, schematic diagram highlighting that *Gna15* belongs to the Gα_q/Gα_{11} family of α-subunits. *B*, migration plots of WT and *Gna15*$^{-/-}$ macrophages in a chemotactic complement C5a gradient. *C*, 200 × 300-μm snapshot of WT and *Gna15*$^{-/-}$ macrophages in a chemotactic complement C5a gradient. *D*, summary box plots of cell velocity and chemotactic efficiency (chemotaxis index), calculated by dividing the displacement along the *y* axis by the cumulative distance migrated. *n.s.*, not significant; Mann–Whitney *U* test ($n = 75$ per group; three independent experiments).

able for the spatial and temporal regulation Rho GTPases and the biasing of protrusions toward higher complement C5a concentrations.

The role of Ca^{2+} transients in chemotaxis is controversial (see Artemenko *et al.* (3)). We found that complement C5a-mediated lamellipodial membrane protrusions were not impaired by sequestration of intracellular Ca^{2+}. Moreover, we confirmed that C5aR-Gα_{15} signaling, which activates PLC-β, almost completely accounts for complement C5a-induced Ca^{2+} signaling, although both lamellipodial cell spreading and chemotaxis were intact in macrophages lacking Gα_{15}. Similar to complement C5a, UTP, an endogenous P2Y$_2$R ligand, induced large Ca^{2+} transients and lamellipodial membrane protrusions. However, we found that P2Y$_2$R-induced Ca^{2+} transients strictly required Gα_q/Gα_{11} and not Gα_{15}. Notably, ATP and UTP are poor long-range chemoattractants for macrophages and neutrophils (15, 34, 35), possibly due to lack of activation of Gα_{i2} or other G$\alpha_{i/o}$ family members by P2Y$_2$Rs and/or rapid degradation of the ligands by ectonucleotidases, such as CD39 and CD73 (36). Although we previously found that a stable (slowly hydrolyzed) analogue of ATP had no chemotactic activity for mouse macrophages (34), Collins *et al.* (35) observed that PLB-985 cells, a human neutrophil-like cell line, migrated transiently (for about 5 min) toward higher concentrations of ATP in a radial gradient generated by UV light–induced uncaging of caged ATP. Thus, ATP may transiently evoke directed migration, whereas complement C5a acts as a durable chemoattractant. We have previously shown that complement C5a induces ATP release, which probably acts as a positive feedback loop because the presence of potato apyrase, which completely degraded ATP, ADP, and adenosine, inhibited complement C5a-mediated chemotaxis (16). Similarly, apyrase was shown to inhibit neutrophil chemotaxis to the chemoattractant fMLP, a formylated tripeptide (15).

C5aR-Gα_{15} signaling as well as ATP/UTP-P2Y$_2$R signaling probably induce lamellipodial membrane protrusions independent of G$\alpha_{i/o}$ family subunits via activation of PLC-β isoforms and depletion of PIP$_2$, as illustrated in Fig. 13. Depletion of PIP$_2$ may cause dissociation of Rac-GAPs and Cdc42-GAPs from the membrane, along the lines described by Li *et al.* (37), thereby promoting increased activity of the Rac subfamily of Rho GTPases, especially Rac1 and Rac2, and Cdc42.

We found that stimulation of WT macrophages with complement C5a increases the levels of active RhoA. However, we did not test whether this effect is lost in *Gna12*/*Gna13* dKO macrophages, and therefore further experiments are required

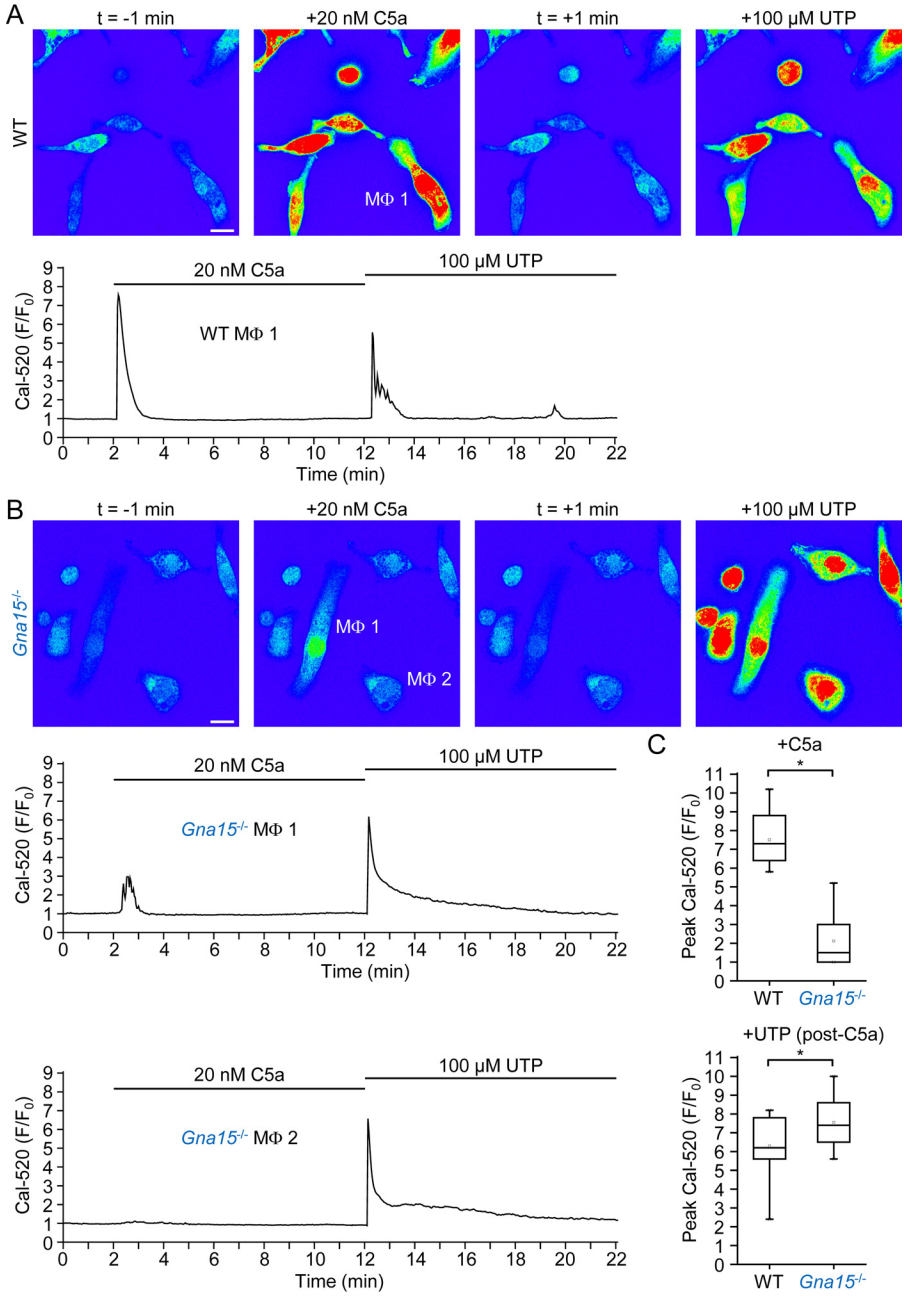

Figure 8. Complement C5a-induced Ca^{2+} transients are largely abolished in *Gna15*-deficient macrophages. *A*, time-lapse images (90 × 90 μm) of WT macrophages loaded with the fluorescent Ca^{2+} indicator Cal-520. Complement C5a and UTP were added as indicated. *Scale bar*, 10 μm. *Below* the series of four images is the intracellular Ca^{2+} signaling corresponding to the macrophage (MΦ) labeled *MΦ1*. Intracellular [Ca^{2+}] is indexed as relative Cal-520 fluorescence intensity (F/F_0), where the measured fluorescence intensity (F) is divided by the resting fluorescence intensity (F_0) after subtracting the background fluorescence intensity at each time point. *B*, time-lapse images (90 μm × 90 μm) of *Gna15*$^{-/-}$ macrophages loaded with Cal-520. Complement C5a and UTP were added as indicated. *Scale bar*, 10 μm. *Below* are traces corresponding to the labeled *Gna15*$^{-/-}$ macrophages (*MΦ1* and *MΦ2*, respectively). *C*, summary peak [Ca^{2+}] data. *, $p < 0.05$; Mann–Whitney *U* test ($n = 14$ for WT (two independent experiments); $n = 30$ for *Gna15*$^{-/-}$ (three independent experiments)).

to determine whether complement C5a receptors couple to $G\alpha_{12}/G\alpha_{13}$. In any case, $G\alpha_{12}/G\alpha_{13}$ signaling does not appear to play a critical role in complement C5a-mediated chemotaxis. Macrophages lacking $G\alpha_{12}/G\alpha_{13}$ exhibited intact chemotaxis, but increased cell velocity and modestly impaired tail retraction. This observation fits in with our previous findings that *Rhoa*/*Rhob* (RhoA/RhoB) dKO macrophages exhibit the same behavior (intact complement C5a-mediated chemotaxis and increased velocity), except *Rhoa*/*Rhob* dKO cells develop much more markedly elongated trailing ends (25). Likewise, human monocytes treated with inhibitors of Rho or its major downstream effector Rho kinase exhibit both normal chemotaxis and elongated trailing ends when migrating on a 2D surface (38). On the contrary, when Rho activity is increased, as in the case of macrophages from mice lacking the RhoGAP Myo9b (21), chemotaxis is impaired, and cell velocity is decreased. The unconventional myosin Myo9b contains an atypical C1 domain (which does not bind to diacylglycerol) (39) and a RhoGAP

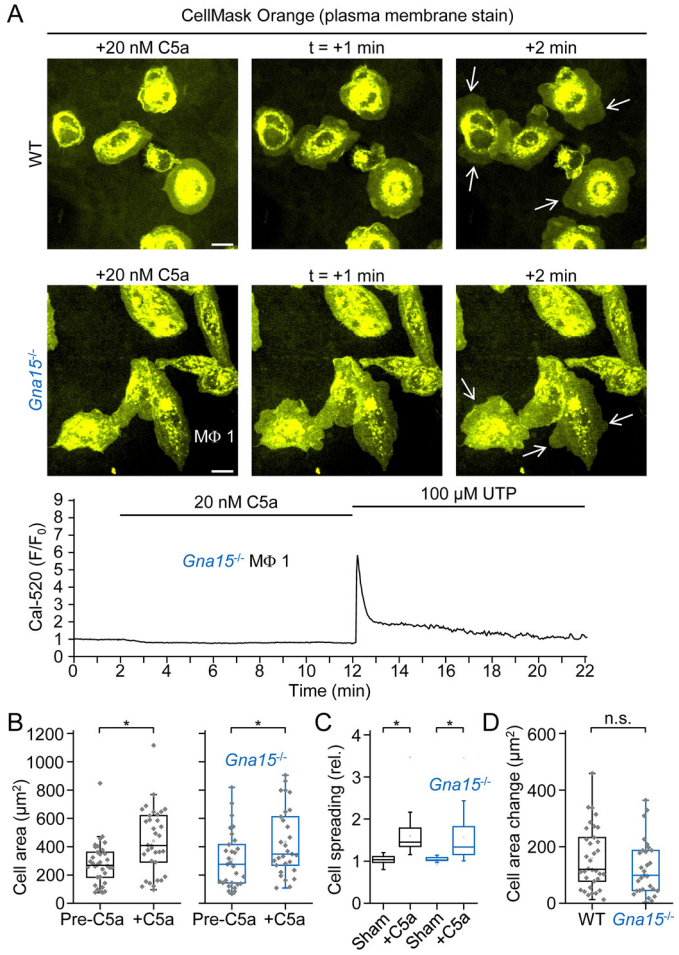

Figure 9. Intact complement C5a-induced lamellipodial membrane spreading and Ca^{2+} transients in *Gna15*$^{-/-}$ macrophages. *A*, time-lapse images (90 × 90 μm) of WT and *Gna15*$^{-/-}$ macrophages stained with the fluorescent plasma membrane marker CellMask Orange and loaded with the fluorescent Ca^{2+} indicator Cal-520. Complement C5a was added as indicated. The *white arrows* indicate examples of lamellipodial membrane protrusion. *Scale bars*, 10 μm. *Below* is the intracellular Ca^{2+} signaling corresponding to the *Gna15*$^{-/-}$ macrophage labeled *MΦ1*. Complement C5a and UTP were added as indicated. Intracellular [Ca^{2+}] is indexed as relative Cal-520 fluorescence intensity (F/F_0), where the measured fluorescence intensity (F) is divided by the resting fluorescence intensity (F_0) after subtracting the background fluorescence intensity at each time point. *B*, box plots of projected cell area before and after application of complement C5a to WT or *Gna15*$^{-/-}$ macrophages. *, $p < 0.05$; Mann–Whitney *U* test. *C*, box plots of relative peak projected cell area after application of ligand-free medium (*Sham*) and complement C5a-containing medium to WT and *Gna15*$^{-/-}$ macrophages. *, $p < 0.05$; Mann–Whitney *U* test ($n = 34$ for WT and $n = 29$ for *Gna15*$^{-/-}$ (three independent experiments)). *D*, box plots of the changes in cell area (prestimulation cell area subtracted from the peak poststimulation cell area) after stimulating WT and *Gna15*$^{-/-}$ macrophages with complement C5a (*n.s.*, not significant; Mann–Whitney *U* test).

domain, but not a pleckstrin homology domain, and probably acts as an actin-binding, motorized inhibitor of Rho at the front of migrating macrophages.

Using lentiviral delivery of siRNA into J774A.1 cells (mouse macrophage cell line), Hwang *et al.* (30) found that deletion of both $G\beta_1$ and $G\beta_2$ eliminated G protein–mediated receptor signaling by all four $G\alpha$ families. Interestingly, in an earlier study, the authors showed that knockdown of $G\beta_2$ alone in J774A.1 cells completely inhibited migration toward complement C5a in transwell assays, and cells showed absent or weak Ca^{2+} responses to complement C5a (29). The authors also found that PTX treatment prevented Ca^{2+} responses. In contrast, we found that complement C5a-induced Ca^{2+} signaling was intact in *Gnb2*$^{-/-}$ macrophages and only modestly reduced in WT cells treated with PTX, whereas *Gna15*$^{-/-}$ macrophages exhibited mostly absent or weak Ca^{2+} responses. However, we observed moderately impaired chemotaxis by *Gnb2*$^{-/-}$ macrophages in a complement C5a gradient. Presumably, $G\beta_1$ partially compensates for loss of $G\beta_2$ in *Gnb2*$^{-/-}$ macrophages. Further studies using macrophages from mice with myeloid-restricted deletion of *Gnb1* would be helpful to explore the relative functions of $G\beta_1$ and $G\beta_2$ in complement C5a-mediated chemotaxis.

In summary, using mouse macrophages lacking specific G protein subunits and real-time imaging assays, we found that (i) the α-subunit $G\alpha_{i2}$ is indispensable, and $G\alpha_{i3}$ is largely redundant, for complement C5a-mediated chemotaxis; (ii) $G\alpha_{15}$ mediates complement C5a-induced Ca^{2+} release, but is dispensable for chemotaxis; (iii) the $G\alpha_{12}/G\alpha_{13}$ family contributes to tail retraction, but is not required for chemotactic navigation; (iv) $G\alpha_q/G\alpha_{11}$ clearly mediate UTP-induced (and ATP-induced) Ca^{2+} release, but autocrine $P2Y_2R$-$G\alpha_q/G\alpha_{11}$ signaling is not important for complement C5a-induced Ca^{2+} release and chemotaxis; (v) deletion of $G\beta_1$ is lethal; (vi) mice lacking $G\beta_2$ are viable; (vii) $G\beta_2$ is important for complement C5a-induced chemotaxis, but not Ca^{2+} signaling; and (viii) complement C5a-induced lamellipodial membrane protrusions persist in the absence of $G\alpha_{i2}$, $G\alpha_{i3}$, $G\alpha_q/G\alpha_{11}$, $G\alpha_{12}/G\alpha_{13}$, $G\alpha15$, or $G\beta_2$.

Experimental procedures

Mice

Gnb1 knockout (*Gnb1*$^{em1(IMPC)Bay}$) mice were generated by the Knockout Mouse Phenotyping Program (KOMP^2) (31) at the Department of Molecular and Human Genetics (Baylor College of Medicine, Houston, TX) using the CRISPR/Cas9 gene-targeting technique. *Gnb2* knockout (C57BL/6NJ-*Gnb2*$^{em1(IMPC)J}$/Mmjax) mice were generated by KOMP^2 at the Jackson Laboratory (Bar Harbor, ME) using CRISPR/Cas9. The knockout allele was produced by injecting Cas9 mRNA and four single guide RNAs (TCCCATTCTTCAGTGCCCCA, ATGGGCAGAATGATAGTACA, TCCCATTCTTCAGTGCCCCA, and ATGATGGGCAGTGCAAGAGA) into C57BL/6NJ-derived fertilized eggs, which were subsequently transferred to pseudopregnant females. The guide RNAs, in combination with the (RNA-guided) DNA endonuclease Cas9, were designed to delete 359 bp in the targeted gene (*Gnb2*), leading to a deletion including exons 3 and 4 and a frameshift after amino acid 19. The frameshift produces a stop codon after coding a further 19 residues. Pups were genotyped using the primer pair (sequences 5′ → 3′) *Gnb2*-F (CCCAAATCCTCTCAGGATGA) and *Gnb2*-R (TGCTTCCCTTTGACCTGAGT), which resulted in a 639-bp PCR product for the WT allele and a 280-bp product for the mutant allele. The generation of *Gnai2* (40) and *Gnai3* (41) knockout mice, which were backcrossed onto a C57BL/6J genetic background (13), have been described previously. *Gnai2*$^{-/-}$ and *Gnai3*$^{-/-}$ mice

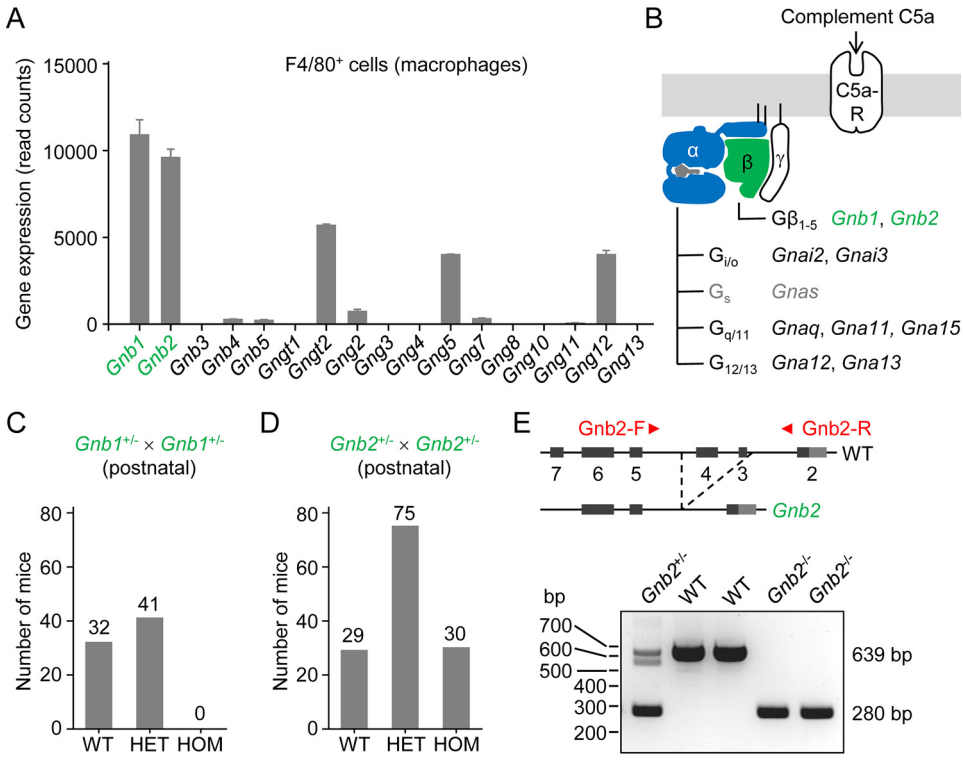

Figure 10. Homozygous deletion of *Gnb1* is lethal, whereas *Gnb2*-deficient mice are viable. *A*, expression levels of Gβ and Gγ subunits in mouse resident peritoneal F4/80$^+$ cells (macrophages). RNA-Seq analysis was performed using RNA isolated from resident peritoneal F4/80$^+$ cells purified by cell sorting (n = 3 mice). *Error bars*, S.E. *B*, schematic diagram highlighting the genes encoding the Gβ-subunits Gβ$_1$ (*Gnb1*) and Gβ$_2$ (*Gnb2*). *C*, homozygous deletion of *Gnb1* is lethal. *D*, homozygous *Gnb2* mutant mice are viable. *E*, schematic diagram of the WT allele and the *Gnb2* knockout allele, generated by CRISPR/Cas9. The forward (Gnb2-F) and reverse (Gnb2-R) primers are indicated by *horizontal red arrowheads*, where the *arrow tip* marks the start of binding. *Below* is an image of an agarose gel depicting the genotyping.

were kindly provided by Johannes Engelbert Gessner (Hannover, Germany). The production of double transgenic mice with floxed (fl) *Gnaq* alleles (*Gnaq*$^{fl/fl}$) and homozygous deletion (−/−) of *Gna11* (*Gna11*$^{-/-}$) has been reported by Wettschureck *et al.* (42). Myeloid-restricted *Gnaq*/*Gna11* double knockout (*Gnaq*$^{fl/fl}$/LysM-Cre/*Gna11*$^{-/-}$) mice were derived by crossing *Gnaq*$^{fl/fl}$/*Gna11*$^{-/-}$ mice with LysM-Cre (B6.129P2-Lyz2$^{tm1(cre)Ifo}$/J) mice (43). Grimm *et al.* (44) recently documented the generation of myeloid-restricted *Gna12*/*Gna13* double knockout (*Gna12*$^{-/-}$/Gna13$^{fl/fl}$/LysM-Cre) mice.

All animal experiments were performed in accordance with the German Animal Welfare Act (Tierschutzgesetz), approved by the local ethics committee of the University of Münster, and conformed to the Guide for the Care and Use of Laboratory Animals of the United States National Institutes of Health.

Isolation of resident peritoneal macrophages

The method, including a video, for isolation of mouse resident peritoneal macrophages has recently been described (45). Mice were killed by an overdose of isoflurane in air, and the peritoneal cavity was lavaged via a 24-gauge plastic catheter (B. Braun, Melsungen, Germany) using 2 × 4.5 ml of ice-cold Hanks' balanced salt solution without Ca^{2+} or Mg^{2+} (14175-046, Gibco). After centrifugation (300 × *g* for 6.5 min), cells were resuspended in bicarbonate-free RPMI 1640 medium containing 20 mM Hepes (R7388-500ML, Sigma–Aldrich, Steinheim, Germany) and modified by supplementation with 10% heat-inactivated fetal calf serum (FCS), 100 units/ml penicillin, and 100 μg/ml streptomycin (pH 7.4). The cells were seeded into fibronectin-coated μ-Slide I chambers or μ-Slide Chemotaxis chambers (Ibidi, Martinsried, Germany) and placed in a humidified incubator (37 °C). After 2 h, μ-Slide I chambers were filled with 1 ml of RPMI 1640 medium containing sodium bicarbonate (R8758-500ML, Sigma–Aldrich), which was modified by the addition of 10% heat-inactivated FCS and antibiotics and incubated overnight at 37 °C with 5% CO_2. Experiments were performed on the stage of an inverted microscope (LSM 510, Zeiss) equipped with a temperature-controlled incubator (incubator XL S, Zeiss) using the same bicarbonate-free RPMI 1640 medium as above.

Time-lapse 2D chemotaxis assays

The 2D chemotaxis assay has been described previously (16, 25), including a video demonstration (47). In brief, cells obtained by peritoneal lavage of a single 3–4-month-old mouse were resuspended in 150–200 μl of medium and diluted to a concentration of 10 × 10^6 cells/ml, and 10 μl of the suspension was seeded into the narrow (1 mm × 2 mm × 70 μm) channel of an uncoated (IbiTreat) μ-Slide Chemotaxis chamber (Ibidi). The narrow channel (observation area) connects two 40-μl reservoirs. Notably, the bottom of the chamber is formed by a thin gas-permeable plastic sheet, which has the same thickness and optical properties as a standard No. 1.5 glass coverslip. After 2 h, the chemotaxis chamber was filled with bicarbonate-free RPMI 1640 medium containing 20 mM Hepes, which was sup-

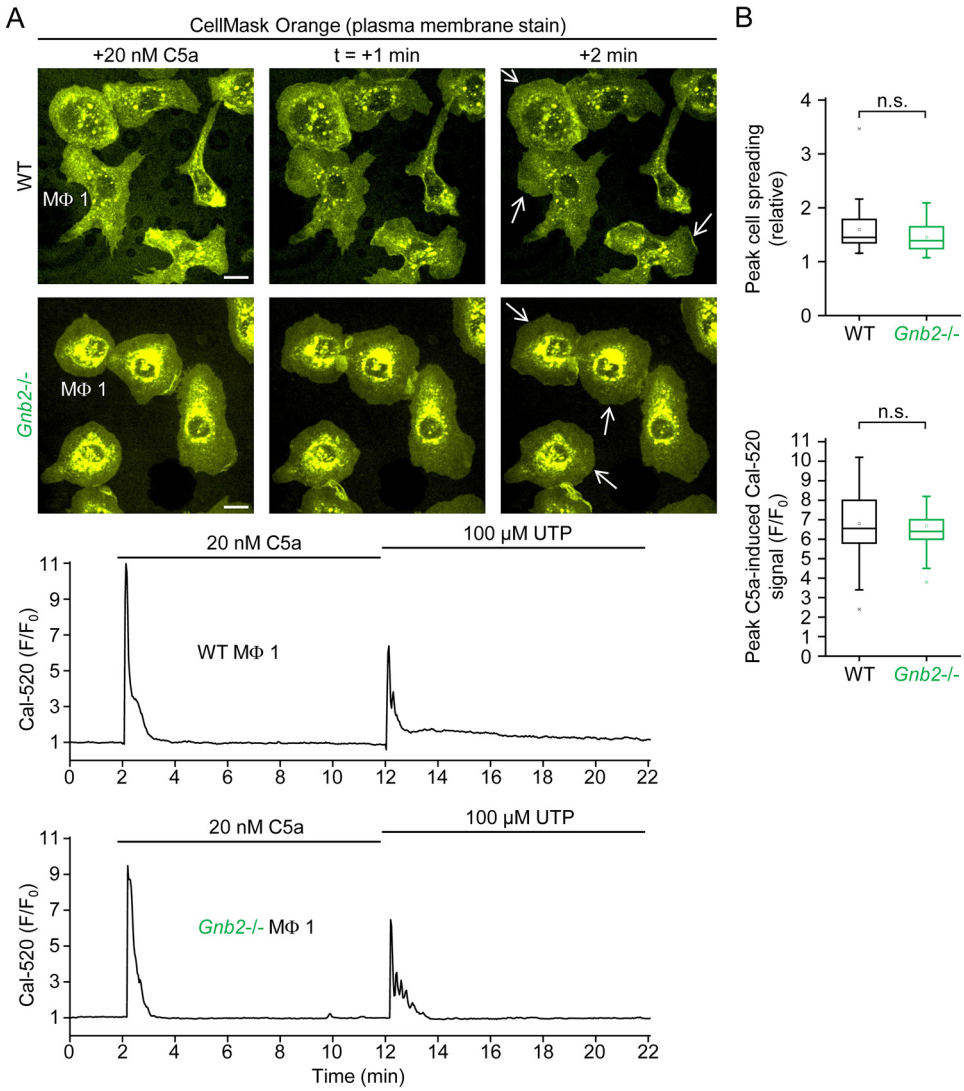

Figure 11. Gnb2$^{-/-}$ macrophages show robust complement C5a-induced cell spreading and Ca^{2+} transients. *A*, time-lapse images (90 × 90 μm) of WT and *Gnb2*$^{-/-}$ macrophages stained with the fluorescent plasma membrane marker CellMask Orange and loaded with the fluorescent Ca^{2+} indicator Cal-520. Complement C5a was added as indicated. The *white arrows* indicate examples of lamellipodial membrane protrusion. *Scale bars*, 10 μm. *Below* the series of cell morphology (CellMask Orange) images is the intracellular Ca^{2+} signaling corresponding to the individual macrophages labeled *MΦ1*. Complement C5a and UTP were added as indicated. Intracellular [Ca^{2+}] is indexed as relative Cal-520 fluorescence intensity (F/F_0), where the measured fluorescence intensity (F) is divided by the resting fluorescence intensity (F_0) after subtracting the background fluorescence intensity at each time point. *B*, summary box plots of peak cell spreading and peak intracellular [Ca^{2+}] induced by complement C5a. *n.s.*, not significant; Mann–Whitney *U* test (n = 52 per group; three independent experiments).

plemented with 10% heat-inactivated FCS, 100 ng/ml lipopolysaccharide, and antibiotics. Next, 15 μl of medium containing chemoattractant (complement C5a) and 0.003% Patent Blue V (blue dye) was drawn into one of the reservoirs. The final concentration of complement C5a was 20 nM. Complement C5a (2150-C5-025, R&D Systems, Abingdon, UK) was reconstituted in PBS containing 0.1% BSA, which had been filtered using a 0.2-μm cellulose acetate membrane (723-2520, Thermo Fisher Scientific). Aliquots were stored at −80 °C. An aluminum heating block maintained at 37 °C was used to keep media and the μ-Slide Chemotaxis chamber warm during the filling procedure. The observation area was imaged by phase-contrast microscopy via a ×10/0.3 objective lens. The blue dye served as a visual indicator of gradient formation. Images were captured every 2 min for 14 h, and cell migration tracks between 6 and 12 h were analyzed with ImageJ (National Institutes of Health) using a cell-tracking plugin and the chemotaxis and migration tool from Ibidi. Twenty-five cells that remained in the field of view were tracked for each chemotaxis assay.

Time-lapse imaging of intracellular [Ca^{2+}] and lamellipodial membrane dynamics

After overnight incubation of resident peritoneal cells, seeded in fibronectin-coated μ-Slide I chambers, in modified RPMI 1640 medium containing sodium bicarbonate, the medium was switched to bicarbonate-free RPMI 1640 medium containing 20 mM Hepes, 1 mM *N*-(2-mercaptopropionyl)glycine (MPG; an antioxidant), 10% heat-inactivated FCS, and antibiotics. The μ-Slide I chambers were placed on an anodized aluminum rack in a dry incubator maintained at 37 °C. Similar to μ-Slide Chemotaxis chambers, the bottom of μ-Slide I

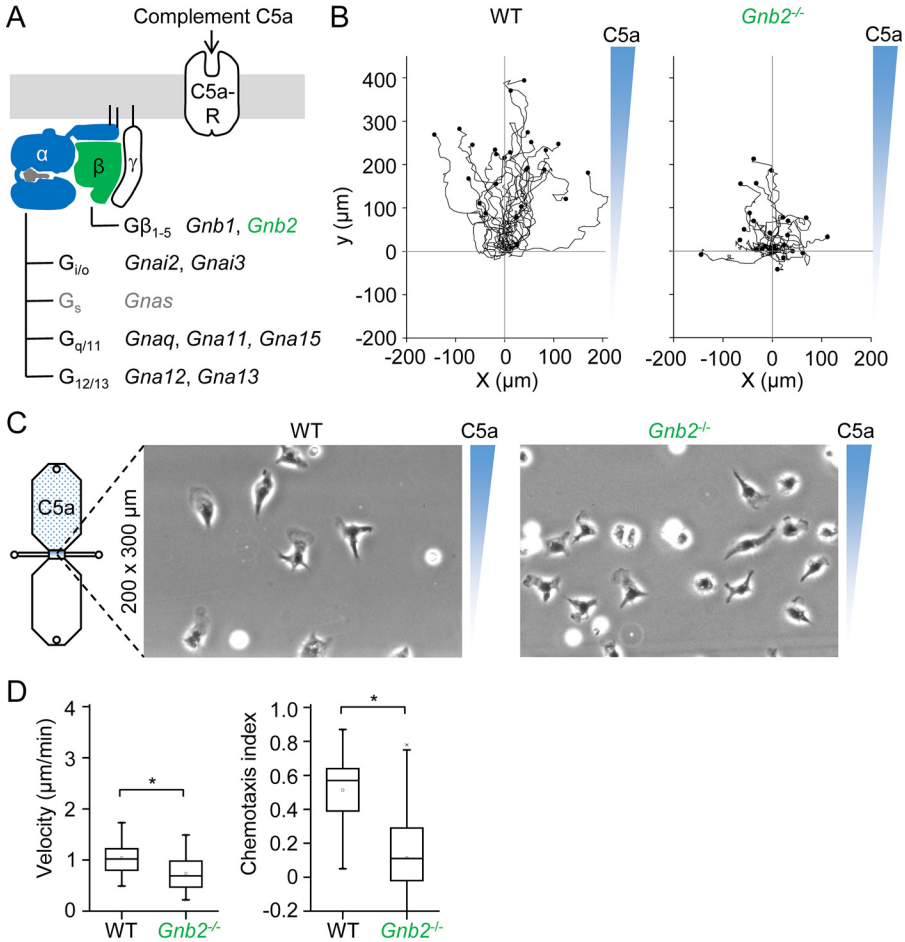

Figure 12. *Gnb2*$^{-/-}$ macrophages have decreased velocity and impaired navigation in a chemotactic complement C5a gradient. *A*, schematic diagram highlighting the Gβ-subunit Gβ_2 (*Gnb2*). *B*, migration plots of WT and *Gnb2*$^{-/-}$ macrophages in a chemotactic complement C5a gradient. *C*, 200 × 300-μm snapshot of WT and *Gnb2*$^{-/-}$ macrophages in a chemotactic complement C5a gradient. *D*, summary box plots of cell velocity and chemotactic efficiency (chemotaxis index), calculated by dividing the displacement along the *y* axis by the cumulative distance migrated. *, $p < 0.05$; Mann–Whitney *U* test ($n = 75$ per group; three independent experiments).

chambers is formed by a gas-permeable plastic coverslip with the same thickness and optical properties as a No. 1.5 coverslip. To image intracellular Ca^{2+}, cells were loaded with the next-generation fluorescent Ca^{2+} indicator Cal-520, using its AM ester form Cal-520/AM (21130, AAT Bioquest, Sunnyvale, CA). A 10 mM stock of Cal-520/AM in anhydrous DMSO (276855-100ML, Sigma–Aldrich) containing 20% (w/v) Pluronic F-127 (Sigma–Aldrich) was prepared by adding 4.53 μl of a 20% solution of Pluronic F-127 in DMSO to a 50-μg aliquot of Cal-520/AM. To prepare a 10 μM loading solution, the 10 mM Cal-520/AM stock solution was diluted 1:1000 in RPMI 1640-Hepes medium containing 1 mM MPG, 10% FCS, antibiotics, and additionally 1 mM probenecid, added from a 200 mM stock solution of the water-soluble sodium salt (P36400, Thermo Fisher Scientific), a competitive blocker of organic anion transporters that reduces the efflux of intracellular anionic fluorescent Ca^{2+} indicators (46). Cells were loaded with Cal-520 by 20-min incubation with 10 μM Cal-520/AM at 37 °C and subsequently washed with RPMI 1640-Hepes medium containing MPG and probenecid.

Lamellipodial membrane dynamics were imaged by either brightfield or fluorescence microscopy. In the latter case, the plasma membrane was stained with CellMask Orange (C10045, Thermo Fisher Scientific), diluted 1:1000 (from a 5 mg/ml stock solution in DMSO) in modified RPMI 1640-Hepes medium or in the above Cal-520 loading solution. Cells were incubated for 10–20 min at 37 °C.

Cells were imaged via the Apochromat TIRF ×60/1.49 (oil-immersion) objective lens of a Nikon Eclipse Ti inverted microscope, which was connected to a spinning-disk confocal system (UltraVIEW Vox 3D live cell imaging system). The system included a Yokogawa (Japan) CSU-X1 spinning-disk scanner, a Hamamatsu (Japan) C9100-50 EM-CCD camera (1000 × 1000 pixels), and Volocity software. Cal-520 was excited with a 488-nm laser, whereas CellMask Orange was excited via a 561-nm laser. Images were captured (at a fixed focus level) using 2 × 2 binning (giving 500 × 500 pixels/image) at a rate of 2 s/time point. Alternatively, cells were alternately imaged by brightfield and fluorescence microscopy at a slower rate of 5 s/time point. Focus drift during long recordings was prevented using the Nikon Perfect Focus System, which maintains the position of the coverslip in the *z* axis by reflecting near-IR light (870 nm) and detecting it via a CCD (charge-coupled device) line sensor. The temperature was maintained at 37 °C using an Okolab all-in-one stage incubator (Okolab, Ottaviano, Italy) and an objective lens heating mantle (Scientific Instruments, Farmingdale, NY).

A

Gene deletion	C5a → Ca^{2+}	UTP → Ca^{2+}	C5a-induced spreading	Complement C5a gradient: Polarization	Complement C5a gradient: Cell velocity	Complement C5a gradient: Chemotaxis
Gnai2$^{-/-}$	++	n.d.	++	↓↓	↓↓	↓↓
Gnai3$^{-/-}$	++	n.d.	++	++	↓	++
Gnaq/*Gna11* dKO	++	↓↓	++	++	++	++
Gna12/*Gna13* dKO	++	++	++	++	↑	++
Gna15$^{-/-}$	↓↓	++	++	++	++	++
Gnb1$^{-/-}$ (lethal)	n.d.	n.d.	n.d.	n.d.	n.d.	n.d.
Gnb2$^{-/-}$	++	++	++	++	↓	↓

B

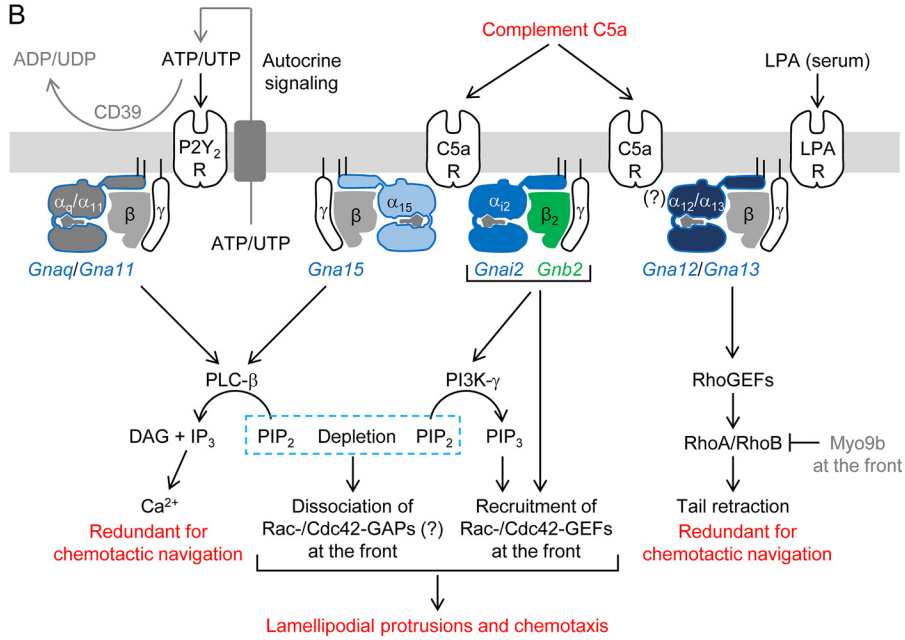

Figure 13. Tabular summary and schematic diagram of G protein subunits involved in transducing complement C5a gradients into directed migration. *A*, tabular summary of results. *B*, schematic summary. C5aRs couple (i) directly to at least two heterotrimeric G proteins formed by $G\alpha_{15}$ and $G\alpha_{i2}$ subunits and possibly also $G\alpha_{12}/G\alpha_{13}$ and $G\alpha i_3$ (not shown) subunits and their respective $G\beta\gamma$ subunits and (ii) indirectly to $G\alpha_q/G\alpha_{11}$-containing heterotrimeric G proteins via autocrine ATP signaling, which stimulates $P2Y_2$Rs. The $G\alpha_{i2}$ subunit is indispensable for chemotaxis and associates with $G\beta_2$-containing, or possibly also $G\beta_1$-containing, $G\beta\gamma$ subunits. $G\alpha_{i2}/G\beta_2\gamma_x$ heterotrimeric G proteins, where *x* is unknown, dissociate into active (GTP-bound) $G\alpha_{i2}$ subunits and $G\beta_2\gamma_x$ dimers following receptor activation by complement C5a. The $G\beta_2\gamma_x$ (or possibly $G\beta_1\gamma_x$) dimers activate PI3Ks, which catalyze the conversion of PIP_2 to PIP_3. PIP_3 is known to recruit pleckstrin homology domain–containing Rac- and Cdc42-GEFs to the membrane. Activation of $G\alpha_{15}$-containing heterotrimeric G proteins directly by complement C5a, as well as indirect activation of $G\alpha_q/G\alpha_{11}$-containing heterotrimeric G proteins via autocrine ATP and UTP signaling, increases the activity of PLC-β isoforms, which catalyze the hydrolysis of PIP_2 to inositol IP_3 and diacylglycerol. IP_3 induces Ca^{2+} release from the endoplasmic reticulum, but this Ca^{2+} signal is largely redundant for lamellipodial membrane protrusions and chemotaxis. However, we speculate that depletion of PIP_2 by PLC-β isoforms and PI3Ks contributes to the formation of lamellipodial membrane protrusions by promoting the dissociation of Rac– and Cdc42-GTPase–activating proteins (GAPs). We speculate that activation of $G\alpha_{12}/G\alpha_{13}$ by complement C5a-C5aR signaling, which remains to be confirmed, increases the activity of the monomeric (small) G proteins RhoA and RhoB via RhoGEFs. Activated (GTP-bound) RhoA and RhoB promote actomyosin-dependent retraction of the trailing end of migrating cells, whereas the RhoGAP Myo9b is thought to inhibit RhoA and RhoB at the front of cells. Extracellular ATP and UTP stimulate $P2Y_2$Rs. ATP, but not UTP, additionally activates P2X receptors (not shown), ligand-gated cation channels. ATP and UTP are rapidly degraded by surface ectonucleotidases, such as CD39, to form ligands for other purinergic receptors (not shown).

The ligands complement C5a and UTP were applied to one of the two reservoirs of a μ-Slide I chamber to induce rapid medium exchange in the 100-μl channel seeded with macrophages. Highly purified (>99%) UTP (R0471, Thermo Fisher Scientific) was added from a 100 mM aqueous solution (pH 7.3–7.5). After application of a ligand or ligand-free medium (in a sham experiment), a second ligand could be applied after aspirating excess medium from the reservoirs flanking the 100-μl channel.

Flow cytometry and cell sorting

Freshly isolated mouse resident peritoneal cells were stained with Alexa Fluor 488–conjugated anti-F4/80 antibodies and resuspended in autoMACS running buffer (Miltenyi Biotec, Bergisch Gladbach, Germany), which contains PBS, 2 mM EDTA, and 0.5% BSA. Purification of F4/80$^+$ cells (mouse macrophages) was performed using a BD FACSAria II (or FACSAria III) cell sorter (BD Biosciences). Recovered cells were centrifuged at 300 × *g* for 5 min, and the supernatant was removed before proceeding to RNA isolation.

RNA isolation and RNA-Seq analysis

Total RNA of purified mouse resident peritoneal F4/80$^+$ cells (macrophages) was isolated by solid-phase extraction using a Direct-zol^{TM} RNA MicroPrep kit (Zymo Research, Freiburg, Germany) according to the manufacturer's instruc-

tions. Briefly, we lysed the pelleted cells with 300 μl of TRIzol (Thermo Fisher Scientific), added 300 μl of analytical (100%) ethanol, and transferred the mixture into a Zymo-Spin™ IC column inserted into a collection tube. Following wash steps, as well as DNase treatment for 15 min, involving several centrifugations at 12,000 × *g*, purified total RNA was captured in a silica column. Using RNase-free water, concentrated RNA was eluted from the silica column and collected in a DNase-/RNase-free safe-lock tube. Isolated RNA samples were tested for integrity using RNA ScreenTape (Agilent Technologies, Santa Clara, CA) and stored at −80 °C.

Next-generation sequencing was performed using a NextSeq 500 Sequencing System (Illumina, San Diego, CA). Samples were prepared using a TruSeq ×RNA sample preparation kit (Illumina), which involved the following steps: purification and fragmentation of mRNA, first- and second-strand cDNA synthesis, end repair, adenylation of 3′ ends, ligation with adaptors, and PCR amplification. RNA-Seq data were analyzed using the Tuxedo suite, an open access set of applications for ultrafast alignment of short reads to the genome, recognition of splice junctions, and differential expression analysis.

G-LISA assay for active RhoA

Levels of active RhoA (RhoA-GTP) were measured using a colorimetric RhoA G-LISA activation assay kit (catalog no. BK124, Cytoskeleton, Denver, CO), according to the elaborate instruction manual. The microplate was shaken at a speed of 400 rpm using Fisherbrand™ microplate shakers (15504070, Fisher), one of which was placed in a cool room (4 °C). Mouse bone marrow–derived macrophages were used instead of peritoneal macrophages to provide sufficient lysates for the assays. Femurs from each mouse were fractured with a scalpel blade at the mid-diaphysis level, and bone marrow cells were flushed out of each fragment using 5 ml of RPMI 1640-Hepes medium containing 10% heat-inactivated FCS and antibiotics, injected via a bent (L-shaped) 23-gauge syringe needle. The isolated cells were pipetted up and down to reduce clumping and transferred into a second 50-ml polypropylene tube via a 70-μm cell strainer. Next, the tube was centrifuged at 300 × *g* for 10 min, and the pellet was resuspended in red blood cell lysing buffer (R7757, Sigma) for 5 min, followed by centrifugation at 300 × *g* for 5 min. After aspiration of the supernatant, the pellet was resuspended in 30 ml of RPMI 1640-Hepes medium containing 10% heat-inactivated FCS and antibiotics, which was supplemented with nonessential amino acids and 15 ng/ml recombinant mouse macrophage colony–stimulating factor (416-ML-010, R&D Systems). The suspension was pipetted into a Teflon bag (PermaLife PL30, OriGen, Biomed Europe), such that each Teflon bag contained cells from a single mouse, and incubated at 37 °C with 5% CO_2 for 6 days. The Teflon bag was placed in ice for 30 min, and the cells, resuspended by shaking and massaging, were poured into a 50-ml tube. The tube was centrifuged at 300 × *g* for 10 min, and the pellet was resuspended in RPMI 1640-Hepes medium containing 10% heat-inactivated FCS and antibiotics and seeded into 35-mm round culture dishes. After a 1.5-h incubation at 37 °C in a CO_2-free incubator, the medium was switched to RPMI 1640 medium containing sodium bicarbonate, 10% heat-inactivated FCS, and antibiotics and incubated overnight at 37 °C with 5% CO_2. Stimulation of cells and the harvesting of lysates were performed after switching back to Hepes-containing medium and allowing at least 1 h of equilibration time.

Statistics

The nonparametric Mann–Whitney *U* test or Kruskal–Wallis one-way analysis of variance on ranks was used to test for statistical differences at the 0.05 level of significance. Post hoc multiple comparisons were made using the Bonferroni correction. Statistical analyses were performed using Origin 2020 (OriginLab) or earlier versions, and data are presented as box plots or mean ± S.E., unless stated otherwise.

Data availability

All data are contained within the article.

Author contributions—E. v. d. B., S. W., and P. J. H. formal analysis; E. v. d. B., B. A., M. H., and P. J. H. investigation; M. H. visualization; A. C. B. and P. J. H. writing-original draft; N. W., G. I., and T. M. W. resources; P. J. H. conceptualization; P. J. H. data curation; P. J. H. supervision; P. J. H. funding acquisition; P. J. H. methodology; P. J. H. project administration.

Funding and additional information—This work was supported by Deutsche Forschungsgemeinschaft (DFG) Grant HA 3271/3-2 (to P. J. H.). T. M. W. is supported by NCI, National Institutes of Health, Grant CA192381. The content is solely the responsibility of the authors and does not necessarily represent the official views of the National Institutes of Health.

Conflict of interest—The authors declare that they have no conflicts of interest with the contents of this article.

Abbreviations—The abbreviations used are: GPCR, G protein–coupled receptor; C5aR, complement C5a receptor; PTX, pertussis toxin; AM, acetoxymethyl; dKO, double knockout; ER, endoplasmic reticulum; PLC-β, phospholipase C-β; IP_3, inositol 1,4,5-trisphosphate; PIP_2, phosphatidylinositol 4,5-bisphosphate; PI3K, phosphoinositide 3-kinase; PIP_3, phosphatidylinositol 3,4,5-trisphosphate; 2D, two-dimensional; FCS, fetal calf serum; MPG, *N*-(2-mercaptopropionyl)glycine; $P2Y_2R$, $P2Y_2$ receptor; GEF, guanine nucleotide exchange factor; GAP, GTPase–activating protein.

References

1. Leber, T. (1888) Ueber die Entstehung der Entzündung und die Wirkung der entzündungserregenden Schädlichkeiten. *Fortschritte der Medizin* **6,** 460–464
2. Lämmermann, T., Afonso, P. V., Angermann, B. R., Wang, J. M., Kastenmüller, W., Parent, C. A., and Germain, R. N. (2013) Neutrophil swarms require LTB4 and integrins at sites of cell death *in vivo*. *Nature* **498,** 371–375 CrossRef Medline
3. Artemenko, Y., Lampert, T. J., and Devreotes, P. N. (2014) Moving towards a paradigm: common mechanisms of chemotactic signaling in *Dictyostelium* and mammalian leukocytes. *Cell. Mol. Life Sci.* **71,** 3711–3747 CrossRef Medline
4. Xiong, Y., Huang, C. H., Iglesias, P. A., and Devreotes, P. N. (2010) Cells navigate with a local-excitation, global-inhibition-biased excitable network. *Proc. Natl. Acad. Sci. U.S.A.* **107,** 17079–17086 CrossRef Medline

5. Huang, C. H., Tang, M., Shi, C., Iglesias, P. A., and Devreotes, P. N. (2013) An excitable signal integrator couples to an idling cytoskeletal oscillator to drive cell migration. *Nat. Cell Biol.* **15,** 1307–1316 CrossRef Medline
6. Arai, H., and Charo, I. F. (1996) Differential regulation of G-protein-mediated signaling by chemokine receptors. *J. Biol. Chem.* **271,** 21814–21819 CrossRef Medline
7. Kuang, Y., Wu, Y., Jiang, H., and Wu, D. (1996) Selective G protein coupling by C-C chemokine receptors. *J. Biol. Chem.* **271,** 3975–3978 CrossRef Medline
8. Wettschureck, N., and Offermanns, S. (2005) Mammalian G proteins and their cell type specific functions. *Physiol. Rev.* **85,** 1159–1204 CrossRef Medline
9. Meade, B. D., Kind, P. D., Ewell, J. B., McGrath, P. P., and Manclark, C. R. (1984) *In vitro* inhibition of murine macrophage migration by *Bordetella pertussis* lymphocytosis-promoting factor. *Infect. Immun.* **45,** 718–725 CrossRef Medline
10. Meade, B. D., Kind, P. D., and Manclark, C. R. (1985) Altered mononuclear phagocyte function in mice treated with the lymphocytosis promoting factor of *Bordetella pertussis*. *Dev. Biol. Standard.* **61,** 63–74 Medline
11. Kehrl, J. H. (2016) The impact of RGS and other G-protein regulatory proteins on $G\alpha_i$-mediated signaling in immunity. *Biochem. Pharmacol.* **114,** 40–52 CrossRef Medline
12. Zarbock, A., Deem, T. L., Burcin, T. L., and Ley, K. (2007) $G\alpha_{i2}$ is required for chemokine-induced neutrophil arrest. *Blood* **110,** 3773–3779 CrossRef Medline
13. Wiege, K., Le, D. D., Syed, S. N., Ali, S. R., Novakovic, A., Beer-Hammer, S., Piekorz, R. P., Schmidt, R. E., Nürnberg, B., and Gessner, J. E. (2012) Defective macrophage migration in $G\alpha_{i2}$- but not $G\alpha_{i3}$-deficient mice. *J. Immunol.* **189,** 980–987 CrossRef Medline
14. Davignon, I., Catalina, M. D., Smith, D., Montgomery, J., Swantek, J., Croy, J., Siegelman, M., and Wilkie, T. M. (2000) Normal hematopoiesis and inflammatory responses despite discrete signaling defects in $G\alpha_{15}$ knockout mice. *Mol. Cell. Biol.* **20,** 797–804 CrossRef Medline
15. Chen, Y., Corriden, R., Inoue, Y., Yip, L., Hashiguchi, N., Zinkernagel, A., Nizet, V., Insel, P. A., and Junger, W. G. (2006) ATP release guides neutrophil chemotaxis via P2Y2 and A3 receptors. *Science* **314,** 1792–1795 CrossRef Medline
16. Kronlage, M., Song, J., Sorokin, L., Isfort, K., Schwerdtle, T., Leipziger, J., Robaye, B., Conley, P. B., Kim, H. C., Sargin, S., Schön, P., Schwab, A., and Hanley, P. J. (2010) Autocrine purinergic receptor signaling is essential for macrophage chemotaxis. *Sci. Signal.* **3,** ra55 CrossRef Medline
17. Li, X. X., Lee, J. D., Kemper, C., and Woodruff, T. M. (2019) The complement receptor C5aR2: a powerful modulator of innate and adaptive immunity. *J. Immunol.* **202,** 3339–3348 CrossRef Medline
18. Zengel, P., Nguyen-Hoang, A., Schildhammer, C., Zantl, R., Kahl, V., and Horn, E. (2011) mu-Slide Chemotaxis: a new chamber for long-term chemotaxis studies. *BMC Cell Biol.* **12,** 21 CrossRef Medline
19. Mangmool, S., and Kurose, H. (2011) $G_{i/o}$ protein-dependent and -independent actions of pertussis toxin (PTX). *Toxins* **3,** 884–899 CrossRef Medline
20. del Rey, A., Renigunta, V., Dalpke, A. H., Leipziger, J., Matos, J. E., Robaye, B., Zuzarte, M., Kavelaars, A., and Hanley, P. J. (2006) Knock-out mice reveal the contributions of P2Y and P2X receptors to nucleotide-induced Ca^{2+} signaling in macrophages. *J. Biol. Chem.* **281,** 35147–35155 CrossRef Medline
21. Hanley, P. J., Xu, Y., Kronlage, M., Grobe, K., Schön, P., Song, J., Sorokin, L., Schwab, A., and Bähler, M. (2010) Motorized RhoGAP myosin IXb (Myo9b) controls cell shape and motility. *Proc. Natl. Acad. Sci. U.S.A.* **107,** 12145–12150 CrossRef Medline
22. Pollard, T. D., and Borisy, G. G. (2003) Cellular motility driven by assembly and disassembly of actin filaments. *Cell* **112,** 453–465 CrossRef Medline
23. Lämmermann, T., and Sixt, M. (2009) Mechanical modes of "amoeboid" cell migration. *Curr. Opin. Cell Biol.* **21,** 636–644 CrossRef Medline
24. Swaney, K. F., Huang, C. H., and Devreotes, P. N. (2010) Eukaryotic chemotaxis: a network of signaling pathways controls motility, directional sensing, and polarity. *Annu. Rev. Biophys.* **39,** 265–289 CrossRef Medline
25. Königs, V., Jennings, R., Vogl, T., Horsthemke, M., Bachg, A. C., Xu, Y., Grobe, K., Brakebusch, C., Schwab, A., Bähler, M., Knaus, U. G., and Hanley, P. J. (2014) Mouse macrophages completely lacking Rho subfamily GTPases (RhoA, RhoB, and RhoC) have severe lamellipodial retraction defects, but robust chemotactic navigation and altered motility. *J. Biol. Chem.* **289,** 30772–30784 CrossRef Medline
26. Wang, S., Chennupati, R., Kaur, H., Iring, A., Wettschureck, N., and Offermanns, S. (2016) Endothelial cation channel PIEZO1 controls blood pressure by mediating flow-induced ATP release. *J. Clin. Invest.* **126,** 4527–4536 CrossRef Medline
27. Wang, S., Iring, A., Strilic, B., Albarrán Juárez, J., Kaur, H., Troidl, K., Tonack, S., Burbiel, J. C., Müller, C. E., Fleming, I., Lundberg, J. O., Wettschureck, N., and Offermanns, S. (2015) $P2Y_2$ and G_q/G_{11} control blood pressure by mediating endothelial mechanotransduction. *J. Clin. Invest.* **125,** 3077–3086 CrossRef Medline
28. Foskett, J. K., White, C., Cheung, K. H., and Mak, D. O. (2007) Inositol trisphosphate receptor Ca^{2+} release channels. *Physiol. Rev.* **87,** 593–658 CrossRef Medline
29. Hwang, J. I., Fraser, I. D., Choi, S., Qin, X. F., and Simon, M. I. (2004) Analysis of C5a-mediated chemotaxis by lentiviral delivery of small interfering RNA. *Proc. Natl. Acad. Sci. U.S.A.* **101,** 488–493 CrossRef Medline
30. Hwang, J. I., Choi, S., Fraser, I. D., Chang, M. S., and Simon, M. I. (2005) Silencing the expression of multiple $G\beta$-subunits eliminates signaling mediated by all four families of G proteins. *Proc. Natl. Acad. Sci. U.S.A.* **102,** 9493–9498 CrossRef Medline
31. Dickinson, M. E., Flenniken, A. M., Ji, X., Teboul, L., Wong, M. D., White, J. K., Meehan, T. F., Weninger, W. J., Westerberg, H., Adissu, H., Baker, C. N., Bower, L., Brown, J. M., Caddle, L. B., Chiani, F., *et al.* (2016) High-throughput discovery of novel developmental phenotypes. *Nature* **537,** 508–514 CrossRef Medline
32. Okae, H., and Iwakura, Y. (2010) Neural tube defects and impaired neural progenitor cell proliferation in $G\beta1$-deficient mice. *Dev. Dyn.* **239,** 1089–1101 CrossRef Medline
33. Boyden, S. (1962) The chemotactic effect of mixtures of antibody and antigen on polymorphonuclear leucocytes. *J. Exp. Med.* **115,** 453–466 CrossRef Medline
34. Isfort, K., Ebert, F., Bornhorst, J., Sargin, S., Kardakaris, R., Pasparakis, M., Bähler, M., Schwerdtle, T., Schwab, A., and Hanley, P. J. (2011) Real-time imaging reveals that P2Y2 and P2Y12 receptor agonists are not chemoattractants and macrophage chemotaxis to complement C5a is phosphatidylinositol 3-kinase (PI3K)- and p38 mitogen-activated protein kinase (MAPK)-independent. *J. Biol. Chem.* **286,** 44776–44787 CrossRef Medline
35. Collins, S. R., Yang, H. W., Bonger, K. M., Guignet, E. G., Wandless, T. J., and Meyer, T. (2015) Using light to shape chemical gradients for parallel and automated analysis of chemotaxis. *Mol. Syst. Biol.* **11,** 804 CrossRef Medline
36. Linden, J., Koch-Nolte, F., and Dahl, G. (2019) Purine release, metabolism, and signaling in the inflammatory response. *Annu. Rev. Immunol.* **37,** 325–347 CrossRef Medline
37. Li, X., Edwards, M., Swaney, K. F., Singh, N., Bhattacharya, S., Borleis, J., Long, Y., Iglesias, P. A., Chen, J., and Devreotes, P. N. (2018) Mutually inhibitory Ras-PI(3,4)P2 feedback loops mediate cell migration. *Proc. Natl. Acad. Sci. U.S.A.* **115,** E9125–E9134 CrossRef Medline
38. Bzymek, R., Horsthemke, M., Isfort, K., Mohr, S., Tjaden, K., Müller-Tidow, C., Thomann, M., Schwerdtle, T., Bähler, M., Schwab, A., and Hanley, P. J. (2016) Real-time two- and three-dimensional imaging of monocyte motility and navigation on planar surfaces and in collagen matrices: roles of Rho. *Sci. Rep.* **6,** 25016 CrossRef Medline
39. Das, J., and Rahman, G. M. (2014) C1 domains: structure and ligand-binding properties. *Chem. Rev.* **114,** 12108–12131 CrossRef Medline
40. Rudolph, U., Finegold, M. J., Rich, S. S., Harriman, G. R., Srinivasan, Y., Brabet, P., Boulay, G., Bradley, A., and Birnbaumer, L. (1995) Ulcerative colitis and adenocarcinoma of the colon in G alpha i2-deficient mice. *Nat. Genet.* **10,** 143–150 CrossRef Medline
41. Jiang, M., Spicher, K., Boulay, G., Martín-Requero, A., Dye, C. A., Rudolph, U., and Birnbaumer, L. (2002) Mouse gene knockout and knockin strategies in application to alpha subunits of G_i/G_o family of G proteins. *Methods Enzymol.* **344,** 277–298 CrossRef Medline

42. Wettschureck, N., Rütten, H., Zywietz, A., Gehring, D., Wilkie, T. M., Chen, J., Chien, K. R., and Offermanns, S. (2001) Absence of pressure overload induced myocardial hypertrophy after conditional inactivation of $G\alpha_q/G\alpha_{11}$ in cardiomyocytes. *Nat. Med.* **7,** 1236–1240 CrossRef Medline
43. Clausen, B. E., Burkhardt, C., Reith, W., Renkawitz, R., and Förster, I. (1999) Conditional gene targeting in macrophages and granulocytes using LysMcre mice. *Transgenic Res.* **8,** 265–277 CrossRef Medline
44. Grimm, M., Tischner, D., Troidl, K., Albarrán Juárez, J., Sivaraj, K. K., Ferreirós Bouzas, N., Geisslinger, G., Binder, C. J., and Wettschureck, N. (2016) S1P2/G12/13 signaling negatively regulates macrophage activation and indirectly shapes the atheroprotective B1-cell population. *Arterioscler. Thromb. Vasc. Biol.* **36,** 37–48 CrossRef Medline
45. Horsthemke, M., Wilden, J., Bachg, A. C., and Hanley, P. J. (2018) Time-lapse 3D imaging of phagocytosis by mouse macrophages. *J. Vis. Exp.* CrossRef Medline
46. Di Virgilio, F., Steinberg, T. H., and Silverstein, S. C. (1990) Inhibition of Fura-2 sequestration and secretion with organic anion transport blockers. *Cell Calcium* **11,** 57–62 CrossRef Medline
47. van den Bos, E., Walbaum, S., Horsthemke, M., Bachg, A. C., and Hanley, P. J. (2020) Time-lapse imaging of mouse macrophage chemotaxis. *J. Vis. Exp.* CrossRef Medline